Urban street canyons: Coupling dynamics, chemistry and within-canyon chemical processing of emissions

Bright, Vivien Bianca; Bloss, William James; Cai, Xiaoming

DOI:
10.1016/j.atmosenv.2012.10.056

Document Version
Peer reviewed version

Citation for published version (Harvard):
Bright, VB, Bloss, WJ & Cai, X 2013, 'Urban street canyons: Coupling dynamics, chemistry and within-canyon chemical processing of emissions', *Atmospheric Environment*, vol. 68, pp. 127-142.
https://doi.org/10.1016/j.atmosenv.2012.10.056

Urban street canyons: coupling dynamics, chemistry and within-canyon chemical processing of emissions

Vivien Bianca Bright, William James Bloss*, Xiaoming Cai

School of Geography, Earth & Environmental Sciences, University of Birmingham, Edgbaston, Birmingham B15 2TT, UK

Abstract

Street canyons, formed by rows of buildings in urban environments, are associated with high levels of atmospheric pollutants emitted primarily from vehicles, and substantial human exposure. The street canyon forms a semi-enclosed environment, within which emissions may be entrained in a re-circulatory system; chemical processing of emitted compounds alters the composition of the air vented to the overlying boundary layer, compared with the primary emissions. As the prevailing atmospheric chemistry is highly non-linear, and the canyon mixing and predominant chemical reaction timescales are comparable, the combined impacts of dynamics and chemistry must be considered to quantify these effects. Here we report a model study of the coupled impacts of dynamical and chemical processing upon the atmospheric composition in a street canyon environment, to assess the impacts upon air pollutant levels within the canyon, and to quantify the extent to which within-canyon chemical processing alters the composition of canyon outflow, in comparison to the primary emissions within the canyon. A new model for the simulation of street canyon atmospheric chemical processing has been developed, by integrating an existing Large-Eddy Simulation (LES) dynamical model of canyon atmospheric motion with a detailed chemical reaction mechanism, a Reduced Chemical Scheme (RCS) comprising 51 chemical species and 136 reactions, based upon a subset of the Master Chemical Mechanism (MCM). The combined LES-RCS model is used to investigate the combined effects of mixing and chemical processing upon air quality within an idealised street canyon. The effect of the combination of dynamical (segregation) and chemical effects is determined by comparing the outputs of the full LES-RCS canyon model with those obtained when representing the canyon as a zero-dimensional box model (i.e. assuming mixing is complete and instantaneous). The LES-RCS approach predicts lower (canyon-averaged) levels of NO_x, OH and HO_2, but higher levels of O_3, compared with the box model run under identical chemical and emissions conditions. When considering the level of chemical detail implemented, segregation effects were found to reduce the error introduced by simplifying the reaction mechanism. Chemical processing of emissions within the canyon leads to a significant increase in the O_x flux from the canyon into the overlying boundary layer, relative to primary emissions, for the idealised case considered here. These results demonstrate that within-canyon atmospheric chemical processing can substantially alter the concentrations of pollutants injected into the urban canopy layer, compared with the raw emission rates within the street canyon. The extent to which these effects occur is likely to be

dependent upon the nature of the domain (canyon aspect ratio), prevailing meteorology and emission / pollution scenario considered.

Keywords: Street Canyons; Air Pollution; Large-eddy simulation; NOx; Ozone

1. Introduction

Urban street canyons, formed by parallel rows of buildings enclosing a vehicular roadway, represent a unique atmospheric environment. Street canyons are commonly the location of substantial primary pollutant emissions, usually dominated by traffic sources. They are also locations where substantial receptor exposure occurs, for pedestrians, road-users and occupants of adjacent buildings which may source their ventilation from the canyon environment. The semi-enclosed form of many urban street canyons can give rise to re-circulatory air flow, reducing the ventilation of the canyon to the overlying urban boundary layer, and further increasing air pollution levels, to potentially harmful levels with serious implications for public health, vegetation and the built environment (Vardoulakis et al., 2003). Atmospheric composition within street canyons is determined by a combination of the composition of background air mixed in from above the canyon, vehicle exhaust and other emissions from within the street, and the mixing and chemical processing of pollutants within the canyon. The interaction of these factors determines both the pollutant concentrations experienced within the canyon, their spatial and temporal variation, the extent to which emissions may undergo chemical processing within the canyon prior to their release into the overlying boundary layer. As the atmospheric chemical reaction system which describes the interaction between nitrogen oxides, ozone and organic compounds is highly non-linear, and the timescale of many of the chemical processes is comparable to the timescale of the large-scale canyon circulation and mixing (seconds to minutes), it is necessary to consider both dynamical and chemical effects to understand the abundance and distribution of reactive species within a street canyon. The aim of this work is to investigate this chemical - dynamical coupling on the street canyon scale, and to gain insight into the oxidative nature of such an environment to understand the potential effects upon within-canyon atmospheric composition (and hence pollutant exposure), and how the canyon outflow composition may differ from the primary emissions, as a result of within-canyon chemical processing.

The airflow characteristics of street canyon dynamics are dependent on the overlying wind direction and speed, and the canyon geometry. In the most simple case, when the direction of the prevailing wind is perpendicular to the canyon axis and the street canyon aspect ratio (defined as the ratio of canyon height (H) to canyon width (W)) is unity ($H/W = 1$), skimming flow is observed in which a large proportion of the flow does not enter the canyon and instead skims over the top of buildings (Oke, 1987). This flow regime results in the formation of a large primary canyon vortex (Fig. 1) in which recirculation effectively decouples the canyon atmosphere from the background air above,

resulting in reduced exchange and poor ventilation. As a result, skimming flow is relatively ineffective in removing pollutants from within the canyon (Hunter et al., 1992). Strong intermittency in the street canyon re-circulation was observed using roof level measurements by Louka et al. (2000) who concluded that the mean flow within the canyon was merely a residual of an unsteady turbulent re-circulation. It was proposed that the strong intermittency observed in the recirculation may be due to the intermittent nature of the mechanism that couples the flow within the canyon with that above i.e. the shear layer at roof level (Fig. 1). This provides an effective ventilation mechanism allowing air to escape and efficient mixing to occur when the shear layer moves to an upward position. Such events, known as sweeps and ejections, are the major turbulent processes that govern pollutant removal from street level to the background atmosphere above (Cheng and Liu, 2011).

Primary pollutants such as nitric oxide (NO), nitrogen dioxide (NO_2) and volatile organic compounds (VOCs) are frequently present in significantly higher concentrations within the street canyon when compared to the overlying background atmosphere, as expected considering proximity to (traffic) emission sources. The oxides of nitrogen (NO_x = NO + NO_2), released predominantly in vehicle exhaust, dominate gas phase chemistry in urban environments. In polluted urban air, levels of the hydroxyl radical (OH) are strongly dependent on chemical cycling, which in turn is dependent on levels of NO_x. OH initiated VOC degradation in the presence of NO_x can result in the formation of secondary pollutants such as ozone (O_3). O_3 is of particular concern in terms of canyon atmospheric composition due to its detrimental effects on human health, vegetation, and the built environment. Within such canyons, O_3 levels are often reduced compared with the overlying air (and more generally, within urban regions compared with the surrounding areas) due to titration by primary NO, an effect known as the urban decrement (AQEG, 2009). Under sunlit conditions, NO_x chemistry is governed by the photochemical steady state (PSS) chemistry in which NO, NO_2 and O_3 establish equilibrium. Interactions with peroxy radicals lead to additional NO-to-NO_2 conversion and result in the net production of O_3. As such, it is valuable to assess the extent to which pollutants may be processed prior to their emission into the wider urban atmosphere, in order to gain an insight into the importance of the oxidative environment of the street canyon.

Long lived pollutants such as carbon monoxide (CO) and volatile organic compounds (VOCs) are unlikely to show a substantial variation in concentration within a street canyon due to chemical processing alone, with their distributions governed near-exclusively by canyon dynamics. Chemical processing of NO_x and O_3, which have shorter chemical lifetimes, occurs on similar timescales to those of the key dynamical processes within the urban canopy layer, thereby causing these species to exhibit a marked variation within the canyon. Very short lived species, such as OH and HO_2, with atmospheric lifetimes of seconds, are highly variable within the canyon and respond rapidly to changes in chemical composition on the canyon scale.

Canyon dynamics and composition have been the subject of field measurement campaigns, wind tunnel experiments and numerical modelling investigations. As road traffic represents the dominant emission source within typical street canyons, in situations where a single primary vortex forms, a large gradient of pollutant concentration is observed across the street with the highest concentration of many pollutants evident toward the leeward wall. A number of field studies have shown that the concentration of pollutants on the leeward side of the street can be significantly greater than that on the windward side and that a vertical decrease in concentration on both sides of the street is observed (Baker et al., 2004; Berkowicz et al., 2002; DePaul and Sheih, 1985; Tomlin et al., 2009; Xie et al., 2003). Although important in terms of model validation, field studies are often relatively sparse in terms of their resolution / spatial coverage and can be influenced considerably by the prevailing meteorological conditions and complex geometry of the surrounding urban environment. Reduced scale physical models (wind tunnel experiments) have also been used to study pollutant dispersion and canyon dynamics and have provided evidence for significant horizontal and vertical gradients in the concentration of passive pollutants within and above the canyon (Gromke et al., 2008; Kastner-Klein and Plate, 1999; Pavageau and Schatzmann, 1999; Salizzoni et al., 2009; Tomlin et al., 2009); however scale effects, and the high spatial and temporal resolution of observations required for full understanding, provide substantial opportunity to use numerical models to investigate canyon dynamics and composition.

Model studies focussing on high resolution representation of canyon fluid dynamics and pollutant transport/dispersion processes have utilised Reynolds-Averaged Navier-Stokes (RANS) models such as large-eddy simulation (LES) to simulate canyon turbulent flow and associated pollutant dispersion; a number of these have been reviewed by Li et al. (2006). Most research has involved the simulation of passive pollutant dispersal (Cai et al., 2008; Cheng and Liu, 2011; Li et al., 2008; Li et al., 2009; Liu and Barth, 2002; Liu et al., 2004; Salim et al., 2011; So et al., 2005). In contrast, relatively little attention has been given to modelling the dispersion of reactive pollutants with most practical applications tending to focus on the dispersion of a passive scalar, or including only a limited number of chemical reactions (Baik et al., 2007; Baker et al., 2004; Garmory et al., 2009; Wang and Mu, 2010). Baker et al. (2004) investigated the turbulent dispersion and transport of reactive pollutants within a street canyon using a large-eddy simulation model with very simple NO_x-O_3 titration chemistry (a two-reaction system) applied, to investigate the deviation from PSS arising from dynamical effects. Substantial deviations from the expected bulk photochemical steady state were found, which were quantified as the photostationary state defect (PSSD). The highest values of the PSSD and therefore greatest deviation from chemical equilibrium, were observed well above the canyon ($z/H \approx 1.3$) corresponding the outer extent of the escaping canyon plume – i.e. where polluted canyon air meets less polluted background air flowing over the canyon. A significant variation in the

147 photostationary state defect within the canyon was also found to occur with the highest 'within
148 canyon' values observed downwind of the emission source and toward ground level on the windward
149 wall, due to entrainment of air by the canyon vortex. The lowest values of the passive scalar co-
150 emitted with NO_x were observed in the centre of the canyon vortex. The same limited reaction scheme
151 was subsequently used by Grawe et al. (2007) to investigate the effect of local shading on pollutant
152 concentrations. Baik et al. (2007) used the same simple representation of the photochemistry to study
153 the dispersion of reactive pollutants within the street canyon, using a RANS-based dynamical model.
154 A similar variation in the photostationary state defect was found, with the largest deviation from
155 chemical equilibrium found above roof level where canyon outflow meets background air, and the
156 region closest to chemical equilibrium found to be the within the canyon vortex. The limited
157 chemical mechanisms present in these studies however neglects the impact of more detailed
158 atmospheric chemistry, for example, peroxy-radical mediated NO to NO_2 conversion with associated
159 O_3 (or total oxidant) production, or NO_x removal through formation of reservoir compounds.
160
161 Few studies have investigated the dispersion of reactive pollutants by applying more comprehensive
162 photochemical reaction schemes to dynamical models. Due to limitations in computing power it is
163 not practical to include the full range of chemical species and reactions that occur in the urban
164 atmosphere (even should all such emissions and reactions be known), particularly when combined
165 with computationally expensive dynamical models such as LES. Explicit representation of the
166 oxidation processes taking place within the canyon may contain several thousand chemical species
167 and over 20,000 reactions (Dodge, 2000). Owing to the computational expense of such models it is
168 still impractical to include *near*-explicit chemical schemes (such as the Master Chemical Mechanism
169 – see below) as a true representation of the canyon chemistry. As a result a number of *reduced*
170 chemical mechanisms, including those reviewed by Dodge (2000), have been developed that
171 reasonably accurately represent the chemical environment of urban canyons, and may be effectively
172 and affordably applied to photochemical / dynamical models.
173
174 The work of Garmory et al. (2009) used the Stochastic Fields (SF) method to simulate turbulent
175 reacting flows and the dispersion of reactive scalars within the street canyon. This research applied
176 the same simple chemical scheme as used by Baker et al. (2004), Grawe et al. (2007) and Baik et al.
177 (2007), and utilised a number of statistical methods to characterise atmospheric processing within the
178 canyon. The results of this initial study were in close agreement with those of Baker et al. and Baik et
179 al., with lowest values of the photostationary state defect located within the canyon, and greatest
180 values observed just above roof level, within the mixing layer. In addition to the simple scheme the
181 more detailed Carbon Bond Mechanism (CBM-IV; Gery et al., 1989) was used. Comparing both
182 mechanisms, the effect of segregation was quantified by evaluating the Damköhler number, *Da*,
183 defined as the ratio of the mixing timescale to the chemical timescale. A value of $Da >> 1$ indicates

that the chemistry / dynamical interaction is important and that segregation effects must be accounted for (Garmory et al., 2006; Krol et al., 2000). If *Da* << 1, species become well mixed much more rapidly than their chemical processing timescale, and hence segregation effects are minimal. For intermediate- and long-lived species, including important species such as O_3 and NO, Garmory et al. found the effect of segregation to be minimal; however for a number of the shorter lived radical species this work, using the CBM-IV mechanism, demonstrated significant differences in predicted concentration in the mixing region above the canyon when segregation effects were considered.

A six-species chemical reaction scheme was applied using both box and LES model frameworks by Krol et al. (2000), with a focus upon the larger atmospheric boundary layer scale (rather than the street canyon domain). Akin to Garmory et al. (2009), this research investigated the deviation from chemical equilibrium, as a result of the turbulent nature of the convective boundary layer, in terms of the intensity of segregation. It was found that turbulence inherent in the convective boundary layer results in large concentration fluctuations and that these give rise to a divergence from chemical equilibrium in contrast to that obtained using box model calculations. When species are emitted uniformly the volume averaged concentrations were found to deviate only slightly from the box model concentrations, however when reactive hydrocarbons were emitted non-uniformly (as is likely to occur in reality) segregation effects are increased, with volume averaged LES model results showing that the rate of destruction of reactive hydrocarbons (RH - representing all reactive hydrocarbons and intermediate species) may be reduced by up to 30 % when compared to that calculated using the box model – i.e. the box model dynamical framework substantially underestimates the chemical lifetime of emitted species within the canyon. It was also found that if both the turbulent timescale and the chemical timescale of a compound are comparable, the integrated flux of RH through the RH-OH reaction will be reduced due to the chemistry-turbulence interaction. Pugh et al. (2011) also investigated boundary layer segregation effects using field measurements taken above a tropical rainforest in South-East Asia. The effect of segregation on the reaction between OH and isoprene was determined using high temporal resolution isoprene concentration data. It was found that the reduction in the effective rate constant for the reaction of isoprene with OH due to segregation effects was typically less than 15 %; an intensity of segregation considerably lower than that needed to explain observed inconsistencies between measured and modelled OH concentrations produced by global and box models of atmospheric chemistry in isoprene rich environments (e.g. Lelieveld et al., 2008).

Most recently, Kwak & Baik (2012) reported CFD simulations of street canyon atmospheric composition incorporating the CBM-IV mechanism, and explored the sensitivity of within-canyon ozone levels to perturbations in NOx and VOC emissions. Ozone was found to be negatively correlated with NO_x, reflecting the impact of NO titration dominating over NO_2 photolysis as a source

of ozone; this was characterised as a negatively NO_x-sensitive regime. Kim et al. (2012) report comparison of CFD simulations using the chemical code from the GEOS-Chem model (Bey et al., 2001) with field observations in a street canyon in Guangzhou, China. The model successfully reproduced the observed levels of species which are essentially passive on the canyon timescale (e.g. CO), but substantially overestimated NO (factor of three). In contrast to the work of Garmory et al., Kim et al. found that modelled canyon O_3 levels varied substantially with the chemical mechanism applied – in comparison with the full reaction scheme, application of a reduced mechanism (NO_x-O_3 photostationary steady state only) led to increases in within-canyon O_3 levels of up to 150 %. The importance of within-canyon processing of emissions, the level of chemical detail necessary to satisfactorily account for such processing, and quantification of the resulting pollutant export to the urban atmosphere, remain open questions.

In the present work, we describe the development of a new model combining a validated representation of street canyon dynamics, together with a sufficiently detailed chemical mechanism to fully assess the impacts of chemistry - dynamics coupling upon atmospheric composition and atmospheric oxidation rates within a street canyon regime. This model combines an LES dynamical treatment with a newly developed and computationally affordable chemical mechanism (termed the reduced chemical scheme, RCS). The RCS mechanism itself was developed from a near-explicit chemical mechanism (the Master Chemical Mechanism; Jenkin et al., 1997), and is validated against the MCM (which in turn has been validated against field and chamber observations), under conditions and timescales relevant to the street canyon regime. In contrast to our previous work, (Baker et al., 2004; Grawe et al., 2007) the level of chemical detail incorporated in the RCS allows the within-canyon VOC oxidation, associated net ozone (or oxidant) production, and NO_x removal through conversion to reservoir species, to be evaluated – all processes well known to be of importance in the real atmosphere, but which the more simple chemical mechanisms cannot address. We apply the combined LES-RCS model to evaluate impacts of the combined chemical and dynamical processes upon within-canyon atmospheric composition and its variability (and hence pollutant exposure), and to evaluate how the canyon outflow differs from the primary emissions within the canyon, as a consequence of within-canyon chemical processing. The effects of chemistry and dynamics are separated by comparing the canyon-average results from full LES-RCS simulations, with those performed under identical chemical conditions, using a box model alone (which corresponds to uniform and instantaneous mixing). A representative flux of processed pollutants out of the street canyon into the overlying boundary layer is determined.

2. Development of the reduced chemical scheme (RCS)

2.1 Chemical Mechanism

In order to develop a suitable model to study street canyon atmospheric composition a representation of the chemistry to be applied within the dynamical model is required. To achieve this, a zero-dimensional box model was used as an efficient tool to develop a chemical reaction mechanism which was sufficiently computationally affordable when implemented within the (computationally expensive) LES dynamical model. The most accurate representation of gas-phase tropospheric chemistry can be achieved through the use of near-explicit chemical mechanisms such as the Master Chemical Mechanism (MCM) (Jenkin et al., 1997) or the Generator for Explicit Chemistry and Kinetics of Organics in the Atmosphere (GECKO-A) (Aumont et al., 2005). The MCM v3.1 describes the degradation of 135 volatile organic compounds (VOCs) including the major UK anthropogenic emissions and biogenic species including isoprene and the monoterpenes α- and β-pinene, including over 5,900 chemical species and 13,500 chemical reactions (Bloss et al., 2005; Jenkin et al., 1997; Jenkin et al., 2003; Saunders et al., 2003). The MCM has been evaluated using high quality datasets obtained from experiments carried out in large outdoor environmental reaction chambers and ambient field observations. As the MCM is too computationally expensive to incorporate directly into the LES framework, a subset of the MCM, the Common Representative Intermediates mechanism version CRI v2-R5 (Jenkin et al., 2008; Watson et al., 2008), which includes 19 emitted anthropogenic VOCs to represent full speciation, 196 chemical species and 555 reactions, was used as a starting point for further scheme reduction. The reduced chemical scheme derived from this (hereafter referred to as the RCS) was then compared with the full MCM simulation, the latter providing the standard for RCS evaluation. The reduced form of the CRI has itself been evaluated in comparison to the MCM and other mechanisms, and found to replicate well both integrated ozone production on timescales of days, and (of more relevance here) OH levels on timescales of hours under polluted (industrial) conditions (Emmerson and Evans, 2009).

2.2 Mechanism Development

In order to reduce the CRI v2-R5, the scope of simulations was initially limited to daytime scenarios, allowing night time only chemistry to be removed (parent VOC degradation by NO_3 and inorganic NO_3/NO_y reactions were retained). Further reduction was achieved by eliminating parent compounds, and any unique daughter products, which had little effect on the key chemical intermediates under street canyon conditions, while scaling the abundance of other (parent) compounds to retain the same OH reactivity. The metrics used to assess each simplification were concentrations of OH, NO, NO_2, O_3 and hydroperoxy radical (HO_2), the key criterion being to maintain OH levels within 10 % of those predicted by the (full) MCM using the (full) parent VOC set. The explicit inorganic chemistry from the MCM was fully retained. The initial concentrations of pollutants used in developing the reduced chemical scheme were determined using observations taken during the Tropospheric ORganic CHemistry experiment (TORCH) field campaign carried out in suburban London (Lee et al., 2006), with the NO_x range extended to cover a range from 15 and 513 ppb, to better represent the conditions

that may occur within a street canyon. The number of parent VOCs considered was reduced, using VOC reactivity (with respect to OH) as a proxy for ozone production potential on the short timescales relevant to the street canyon residence time. Physically the OH reactivity of a VOC represents the inverse of the lifetime of OH due to loss by reaction with that species; OH reactivity provides a suitable measure of the overall potential for VOC oxidation and subsequent formation of organic peroxy radicals and hence O_3 formation. The remaining parent VOC abundance was adjusted to maintain the total OH reactivity (Equation 1), at the (observed) value of 3.4 s^{-1} (Lee et al., 2006).

$$k'_{OH} = \sum k_{1(OH+VOC_1)}[VOC]_1 + k_{2(OH+VOC_2)}[VOC]_2 + k_{3(OH+VOC_3)}[VOC]_3 \ldots \quad (1)$$

The final RCS includes 51 chemical species and 136 reactions; with methane and 8 parent non-methane hydrocarbons (NMHCs) included in the mechanism (Table 1: isoprene, ethene, propene, formaldehyde, acetaldehyde, methanol, ethanol and peroxyacetylnitrate).

2.3 Evaluation of the RCS

The accuracy of the RCS was assessed in comparison to the evolution of species concentrations calculated using the full MCM for a single air parcel, initialised using the starting concentrations listed in Table 1. Over a four hour period, the maximum percentage difference in OH between the RCS and the MCM was approximately 6 %, which is within the bounds of the smallest errors associated with the measurement of OH (7 – 16 %) (Heard and Pilling, 2003). For NO, NO_2, O_3 and HO_2 the largest differences between the RCS and the MCM, which occur toward the end of the four hour time period, are 15 %, 7 %, 4 % and 14 % respectively. At the 30 minute time point, more relevant to canyon residence times, smaller differences of 0.4 %, 0.1 %, 0.2 %, 1.1 % were observed respectively, with 0.7 % for OH. The RCS and MCM were also compared under elevated NO_x conditions (NO = 1000 ppb and NO_2 = 120 ppb) which may be experienced within canyons due to proximity to vehicle exhausts. The maximum differences observed over a four hour period were 3 %, 13 %, 16 %, and 4 % for NO, NO_2, O_3 and HO_2 respectively with 12 % for OH. At t = 30 minutes the modelled differences were 0.3 %, 1.7 %, 2.1 %, 3.0 % and 2.4 % for NO, NO_2, O_3, HO_2 and OH respectively. These values are significantly smaller than the uncertainty associated with emissions and with the measurement of such pollutants (Boulter et al., 2009; Lee et al., 2006).

3. Configuration of models used to simulate urban street canyon composition

Two principal approaches are applied here to simulate atmospheric composition and pollutant processing in street canyons. The primary tool is the full LES-RCS model, which represents the most comprehensive treatment of the combined effects of dynamics, chemistry and emissions; the LES-RCS domain included both the street canyon and the overlying boundary layer (described below, section 3.1). The LES-RCS output was compared with simulations in which the street canyon was approximated by a zero-dimensional box model ("Box-RCS"), corresponding to a scenario in which

concentrations are homogeneous (*i.e.* the volume of air is assumed to be instantaneously and completely mixed). In this scenario, the box model corresponds to the within-canyon region ($z/H \leq 1$), and exchange with the overlying boundary layer was parameterised using an exchange velocity expression, as described below.

3.1 Configuration of the LES-RCS model

The LES dynamical model was used to simulate atmospheric motion and turbulent flow in and above an idealised street canyon with an aspect (height/width) ratio of one. The model is based on the Regional Atmospheric Modelling System (RAMS), described in more detail in Cui et al. (2004). The prevailing wind direction in the model remains constant and perpendicular to the canyon axis, which is representative of a worst case scenario from the perspective of pollutant accumulation, in which canyon ventilation is minimal. The wind speed was initially set to zero below the roof level and increased logarithmically to a maximum speed, U_{max}, of 2.5 m s^{-1} at the top of the domain. Mesh resolution in the *x*, *y* directions were Δx = 0.3 m, Δy = 1.0 m respectively. In the *z* direction, Δz = 0.3 m within the canyon and gradually stretched by a factor of 1.15 above roof level (z = 18.0 m) to a maximum of 5.0 m at the top of the domain (z = 94 m). Cyclic boundary conditions were applied to all three velocity components along x- and y-directions. The temperature was defined as 293 K throughout the whole model domain, representative of neutral conditions. Fig. 2a illustrates the street canyon domain included in the LES model, while Fig. 2b shows the developed flow field within and above the canyon. The dynamical part of the LES model for a canyon with an aspect ratio H/W of 1 has been validated by Cui *et al*. (2004), through comparisons of the mean wind and resolved-scale turbulent kinetic energy (TKE) against wind-tunnel experiments, while the scalar part of the model under various H/W ratios has been validated by Cai *et al*. (2008), in which the normalized fluxes were compared with wind-tunnel measurements.

In each experiment, the model was run without chemistry for 30 minutes in order for the turbulent dynamics to reach a quasi-equilibrium state (Cai et al., 2008). At this time, concentrations of all 51 chemical species (initial concentration as listed in Table 1; intermediate and product concentrations as calculated from a 30-minute model integration) were inserted in the whole model domain uniformly. This set of values was also used as the inlet boundary conditions above the upwind building throughout the simulation. At the outlet boundary, the advective condition, $\frac{\partial c_i}{\partial t} + u\frac{\partial c_i}{\partial x} = 0$, was applied to all chemical species, where c_i represents the concentration of species, *i* and *u* is horizontal velocity. For the intermediate- and longer-lived chemical species included in the chemical mechanism, for example, NO, NO_2, O_3 and CO, a timestep of 10^{-2} s was used in the numerical integration, while for shorter lived species such as OH, HO_2 and RO_2 a timestep of 10^{-3} s was

365 employed. These timestep values were empirically chosen to balance the requirement for stable
366 output / convergence against integration time.
367
368 Emissions within the canyon were represented by two line sources centred at 2.5 m to the left and
369 right of the canyon centre, signifying two lanes of traffic. Each of the line sources was considered to
370 have a Gaussian distribution (where σ_x = 3 m and σ_y = 1 m), which were located at 1.0 m above the
371 road as illustrated in Figure 1, and were continuous in nature. The emission rates included in the
372 model were determined using the UK Road Vehicle Emission Factors (2009 - Boulter et al., 2009)
373 and are representative of moderate weekday traffic (1500 vehicles per hour) for an urban road with
374 cars travelling at an average speed of 30 mph. The total emissions for NO, NO_2, CO, ethene (C_2H_4),
375 propene (C_3H_6), formaldehyde (HCHO) and acetaldehyde (CH_3CHO) used were 101, 17, 377, 36, 24,
376 11 and 16 μg m^{-1} s^{-1}, which equate to 900, 100, 3593, 347, 150, 96 and 98 ppb emitted into one LES
377 model cell (0.3 m × 0.3 m × 1 m) per second, respectively. Photolysis frequencies were calculated
378 offline using the Tropospheric Ultraviolet and Visible (TUV) Radiation Model v4.1 (Madronich and
379 Flocke, 1998), using conditions representative of those for a street canyon in Birmingham, UK (52 ^{o}
380 29' N; -1 ^{o}54$^{'}$ W) at 12.00 UTC on 1st August, giving a calculated solar zenith angle of 34^{o}. The
381 ground elevation was specified as 0.12 km and the atmosphere was assumed to be cloud free. A
382 surface albedo of 0.15 was defined i.e. typical of an urban street surface (DFT, 2009; Liu et al., 2011).
383 Photolysis rates were held constant over the modelling period in order to reduce the computational
384 expense once implemented in the LES, reflecting the short residence time (minutes) of a typical street
385 canyon air parcel (Baker et al., 2004; Vardoulakis et al., 2003). Following the initiation of the
386 emissions and chemistry, the combined effects of emission, mixing and chemical processing on
387 atmospheric composition could then be simulated by the LES-RCS model, and the results examined to
388 provide an insight into the processes affecting atmospheric composition over a 180 minute period.
389
390 Using the LES-RCS model, 3-D data was obtained over the period from 30 to 210 minutes at 5 s time
391 intervals. Results were averaged along the *y*-axis over the length of the canyon (L_y - along which the
392 resolved-scale turbulence is homogeneous), across the width of the canyon (the *x*-axis; *W*) and over
393 the height of the canyon (the *z*-axis; *H*) to give a volume averaged (0-D) within-canyon concentration
394 as a function of time, i.e.:

395 $$\overline{c_i}(t) = \frac{1}{W \cdot H \cdot L_y} \int_{-0.5W}^{0.5W} \int_{0}^{H} \int_{0}^{L_y} c_i(x, y, z, t) dx dy dz. \quad (2)$$

396 The LES results were averaged along the length of the canyon in the *y* axis (L_y), across the width of
397 the canyon in the *x* axis (*W*), over the height of the canyon in the z axis (*H*) and averaged over the
398 final hour of the simulation ($150 \leq t \leq 210$ min, i.e. after 30 minutes of dynamical and 120 minutes of

399 chemical spin-up) to give a time and volume averaged within canyon concentration, for comparison
400 with the box-model scenario.

401 $$\overline{c_i} = \frac{1}{W \cdot H \cdot L_y \cdot (t_2 - t_1)} \int_{t_1}^{t_2} \int_{-0.5W}^{0.5W} \int_{0}^{H} \int_{0}^{L_y} c_i(x, y, z, t) dx dy dz dt. \quad (3)$$

402 The LES results were also averaged along the length of the canyon in the y axis (L_y) and over the final
403 60 minutes of the averaging period to give 2-D time averaged concentrations ($150 \leq t \leq 210$ min) i.e.:

404 $$\langle \varphi \rangle (x, z) = \frac{1}{L_y \cdot (t_2 - t_1)} \int_{t_1}^{t_2} \int_{0}^{L_y} \varphi(x, y, z, t) dy dt \,, \quad (4)$$

405 where φ can be w or c_i. Following Eq. (4), $\tilde{\varphi} = \varphi - \langle \varphi \rangle$ represents the resolved fluctuations of φ
406 about $\langle \varphi \rangle$. Thus the following quantities are defined: the resolved-scale vertical turbulent flux,
407 $F_{turb} = \langle \tilde{w} \tilde{c}_i \rangle$, the vertical advective flux, $F_{adv} = \langle w \rangle \langle c_i \rangle$, and total resolved-scale vertical flux
408 $F_{total} = F_{turb} + F_{adv}$. These are 2D quantities showing the spatial pattern of these variables in the x
409 and z domain. For the purposes of analysis, vertical mixing ratio profiles were extracted from the 2-D
410 time averaged concentrations at five sites across the canyon. In addition, the horizontally-averaged
411 vertical profile of the passive scalar's flux inside and above the canyon was derived (Equation 5):

$$F(z) = \frac{1}{W} \int_{-0.5W}^{0.5W} F(x, z) dx. \quad (5)$$

412

413 *3.2 Configuration of the zero-dimensional box-RCS model*

414 As one aim of this work is to compare canyon-average concentrations predicted by the full LES-RCS
415 model using Equation 2, with their equivalents determined using a zero-dimensional box model, under
416 identical chemical and emission conditions, treatment for the exchange between the street canyon and
417 the overlying boundary layer was required. In the case of the LES-RCS model, the modelled domain
418 (Figure 2) includes both within-canyon and above-canyon regions, and so implicitly incorporates
419 exchange between the canyon and the overlying boundary layer. For the box model scenario, mixing
420 with an overlying boundary layer was achieved by implementing a suitable exchange velocity (ω_t)
421 within the model, defined as:

422 $$\omega_t = \frac{F_c}{\bar{c} - c_B} \quad (6)$$

423 where F_c is the pollutant flux F_i at roof level ($z/H = 1$) and the denominator is the difference between
424 the mean concentration within the canyon ($\bar{c}$) and the background concentration above the canyon
425 (c_B). In the case of the box model simulations, the composition of the overlying boundary layer was
426 assumed to be constant, and set equal to the LES-RCS domain inlet composition.

The value of ω_t was determined using LES simulations of a passive scalar (a non-reactive emitted species which is conserved within the model, and whose concentrations are therefore determined by dynamics alone) to evaluate mean rate of exchange between the canyon and boundary layer in the LES simulations. A mean value of $\omega_t = 0.021$ m s^{-1} was determined, averaged over the final hour of the simulation ($150 \leq t \leq 210$ min). Use of a single mean value removes the variability in the LES simulations (arising from periodic sweep / ejection events) – apparent in the comparisons of mean concentrations discussed below. The chemical scheme, photolysis treatment and emissions were identical in the LES-RCS and Box-RCS model cases.

4. Results and discussion

4.1 Spatial variation

Fig. 3 illustrates the mean mixing ratios of the passive scalar (subject solely to dispersion / mixing) and of a number of chemical species, averaged over the final 60 minutes of the 210 minute simulation (logarithmic colour scales for O_3, OH and HO_2). Major features apparent are the primary vortex that spans the canyon and the shear layer at roof level that increases in amplitude and becomes increasingly turbulent downwind, trapping pollutants toward the leeward wall and allowing greater exchange toward the windward wall. Increased levels of NO, NO_2 and the passive scalar are observed within the street canyon compared to the background atmosphere above roof level, as expected. The highest concentrations of these species are found at low level toward the leeward wall, a result of the limited dispersion and chemical processing of emissions before they are transported downwind from their sources located towards the centre of the street. In the case of NO_2, increased levels observed toward the leeward wall at street level arise through secondary formation through reaction of NO with entrained O_3, i.e. through the oxidation of emitted NO, in addition to that emitted directly. HO_x levels are much lower within the canyon than in the background air, with a local maximum in the centre of the vortex, a semi-isolated region of entrained background air. Elevated OH within this region (relative to the periphery of the canyon) primarily reflects a reduced OH sink, in particular reaction with NO – see below.

Fig. 4 illustrates the vertical mixing ratio profiles of O_3, NO, NO_2, OH and HO_2 shown using a logarithmic scale at five across street locations within the canyon ($z/H \leq 2$). The concentrations of O_3, OH and HO_2 increase near roof level on the approach to the less polluted background atmosphere above. The smallest transition between within canyon and background concentrations of all chemical species occurs toward the windward wall due to the increase in exchange of air between the canyon and the background air above in this region associated with the turbulent nature of the shear layer at this point. Towards the leeward wall a sharp contrast exists between the canyon and the background atmosphere, marked by a large change in concentration with height at roof level as pollutants become

effectively trapped by the relatively impermeable shear layer that exists in this region. Fig. 4(a) illustrates a significant change in the concentration of NO and NO_2 across the canyon with the concentration of NO at street level toward the leeward wall more than double (2.3 x) that observed on the windward side, whilst NO_2 levels are over a third higher (1.4 x). The highest mixing ratios of ozone within the canyon are evident toward the windward wall and in particular toward roof level where ozone rich air is brought into the canyon from aloft. Toward the leeward wall the mixing ratios of both NO and NO_2 show a significant decrease with height above roof level where levels rapidly approach those of the background atmosphere. Moving toward the windward wall of the canyon again results in a much more gradual transition between within canyon and the background atmosphere as the influence of the shear layer spans a greater distance in this region causing the air well above the canyon to be mixed with that escaping from within.

The change in mixing ratio of OH and HO_2 is illustrated in Fig. 4(b). Within the canyon the greatest concentrations of both OH and HO_2 are observed toward roof level at the windward wall where concentrations are slightly higher for OH and over a third greater for HO_2 when compared to that at street level toward the leeward wall. OH and HO_2 levels are higher in the centre of the primary canyon vortex. Close to roof level ($z/H \approx 1.1$) toward the leeward wall of the canyon OH and HO_2 approach their background mixing ratios of 0.22 and 1.54 ppt respectively, while these levels are only achieved well above at $z/H \approx 1.5$ on the windward side of the canyon. The reductions in OH and HO_2 within the canyon compared to the background atmosphere are 64 % and 85 % respectively (averaged across the canyon). Mean within canyon levels of NO and NO_2 of 168 and 68 ppb respectively (Table 3) are considerably greater than the overlying urban boundary layer, while within-canyon O_3 levels are on average 11.2 ppb lower than those in the background atmosphere.

Figure 5(a) illustrates the mixing ratio of the sum of organic peroxy radicals (i.e. Σ RO_2, here excluding HO_2) determined by the LES-RCS, averaged over the final 60 minutes of the simulation (logarithmic colour scale). The RO_2 abundance exhibits a similar pattern to that of OH, with a local minimum toward the lower leeward wall and maxima observed within the primary vortex, close to the mixing layer at roof level and toward the windward wall, and a tongue of elevated RO_2 accompanying the entrained air into the vortex on the windward side. To further investigate the importance of HO_x sources and sinks within and above the canyon, the chemical rate of production / loss for OH was evaluated, using time averaged ($150 \leq t \leq 210$ min) reactant concentrations determined for three locations (indicated in Fig. 5a): (V) within the vortex ($z/H = 0.5$, $x/W = 0$), (L) toward the leeward wall ($z/H \approx 0.08$, $x/W \approx -0.3$) and (B) in the background atmosphere above the canyon ($z/H \approx 1.2$, $x/W \approx -0.3$). The change in OH with respect to time is governed by the rate of production and loss, as below (neglecting transport, negligible for OH):

$$\frac{\partial[OH]}{\partial t} = P_{OH} - \sum_X k[OH][X]. \qquad (7)$$

Where P_{OH} is the total rate of production of OH, and $-k$ [OH] [X] represents the chemical loss of OH through reaction with X. The dominant OH chemical production and loss terms for each location (rates of reaction, here expresses in ppt s^{-1}) are given in Table 2. Primary OH production (O_3 photolysis) predictably falls with reduced O_3 abundance from the background into the canyon (NO titration), but comprises a small fraction of the total production rate. NO-driven radical cycling dominates OH production, with a significant (up to 22 %) contribution from HONO photolysis. The lifetime of HONO is comparable to the timescale of the vortex circulation and mixing (photolysis lifetime of 8 minutes), thus HONO must be explicitly considered in understanding OH abundance (cannot be assumed to be in steady state). No heterogeneous sources of HONO were implemented within this model – see discussion below. Going from the background to leeward (within-canyon) locations, the OH sink increases from 2.8 s^{-1} to 96 s^{-1}, a factor of 30, while the dominant OH production rate, HO_2 + NO, increases from 1.1 to 11.7 ppt s^{-1} (total OH production increases by a factor of 8.8); accordingly within-canyon OH levels are much lower than in the overlying boundary layer. The local maximum in OH in the vortex centre arises from the semi-isolated nature of this part of the domain; at the centre, OH production rates are comparable with those at the leeward site (total production rate of 11.5 vs. 13.6 ppt s^{-1}, dominated by HO_2 + NO), but the OH sink is much lower than that directly downwind of the emission source – 61 vs. 96 s^{-1} – and OH levels are correspondingly *ca*. 31 % higher.

Within the street canyon, gas phase chemistry is dominated by NO_x and as such it is often useful to consider the temporal and spatial variation in NO_x levels. The chemical interaction of NO_x with O_3 plays a key role in determining NO_2 levels observed in the urban environment. As a result of this interaction, another useful measure to consider is defined as the total oxidant (O_X = O_3 + NO_2). Considering only NO-NO_2-O_3 reactions, O_X is conserved whilst partitioning between the component forms of O_3 and NO_2 is determined by overall levels of NO_x, O_3 and solar radiation. Figs. 5(b) and (c) illustrate the spatial variation in NO_x and O_X within and above the canyon domain. The mixing ratios of NO_X and O_X are both greater within the canyon (236 and 79 ppb respectively) compared to the background atmosphere where NO_x = 9 ppb and O_X = 50 ppb. The spatial distribution of NO_x (Fig 5(b)) is similar to that of the passive scalar (Fig. 3(d)) demonstrating the effective conservation of NO_x on the canyon residence timescale. The change in mixing ratio of NO_x and O_X with height within the canyon ($0.0 \leq z/H \leq 2.0$) at five sites across the street is illustrated in Fig. 6 using a logarithmic scale. The highest concentration of NO_x occurs at street level toward the leeward wall downwind of the two line emission sources located in the centre of the street. Figs. 5 and 6 also indicate that the lowest levels of O_X occur toward street level on the upper windward wall with the highest concentrations close to street level toward the leeward wall. Elevated O_X in this region arises from the 5 % primary NO_2 emission within the NO_x source term. The lowest ratios of NO_2 to NO (Fig. 5d) occur at street level downwind of the emission sources toward the leeward wall. The

decrease in the NO_2/NO ratio within the canyon primarily reflects the predominance of NO in the primary NO_x emission term. Table 3 illustrates that the ratio of NO_2 to NO is higher for the box model case indicating greater (mean) simulated conversion of NO to NO_2 when dynamical effects are neglected (i.e. assuming instant mixing). This arises as a number of cells within the LES model have very little or no O_3 present (Fig. 3) hence NO to NO_2 conversion is precluded at many locations.

4.2 Atmospheric composition and exchange rate effects

The change in the canyon averaged concentration of the passive scalar over time is compared between the LES and box model results (Fig. 7). Fluctuations in the concentration of the averaged passive scalar inherent in the LES results are caused by large scale variations of the flow and the variable nature of canyon ventilation caused by the unsteady fluctuations in the shear layer at roof level, as observed by Louka et al. (2000) and reproduced by the model. The optimum value of exchange velocity, ω_t, can be determined by minimising the difference between the passive scalar results for the LES and box model. As shown in Fig. 7, for the final 60 minute averaging period a value of ω_t = 0.021m s^{-1} applied to the box model best represents the LES values and is therefore applied to the box model simulations for comparison with canyon averaged LES results of other chemical species.

The sensitivity of the canyon averaged concentrations derived from the box model output to the value of the exchange velocity, ω_t, between the canyon air and the background atmosphere was investigated. The effect of increasing ω_t from 0.021 m s^{-1} to 0.022 m s^{-1} is illustrated in Table 4. This increase in the exchange velocity results in a decrease in mean within canyon averages of NO_x and O_X by 4.5 % and 2 % respectively. The concentration of O_3 increases with ω_t, partially due to an increase in O_3 rich background air entering the canyon from above, and partly due to lower NO levels reducing the titration of O_3 to NO_2. For OH and HO_2, increasing ω_t reduces the modelled levels due to a reduction in the concentration of VOCs, as increased mixing leads to increased ventilation out of the canyon. In the case of the passive scalar, we have $\omega_t \cdot \left(\overline{c} - c_B\right) = constant$, and thus

$$\frac{\overline{c^{(b)}} - c_B}{\overline{c^{(a)}} - c_B} = \frac{\omega_a}{\omega_b}, \quad \text{and} \quad \frac{\overline{c^{(b)}} - \overline{c^{(a)}}}{\overline{c^{(a)}}} \cong -0.045.$$

Whereas for NO_x where $c_B << \overline{c^{(a)}}$ then $\dfrac{\overline{c^{(b)}} - \overline{c^{(a)}}}{\overline{c^{(a)}}} \cong -\dfrac{\omega_b - \omega_a}{\omega_a} = -0.048.$

The similarity of these results (and those in table 4) indicates that (on this timescale) NO_x is approximately passive in nature.

4.3 Temporal changes and segregation effects within the canyon

The variation with time of the spatially averaged 'within canyon' concentrations of a number of species simulated by the LES-RCS model is compared with their equivalents simulated using the box

model (with equal emissions and net external mixing applied) in Fig. 8. Significant differences between the concentrations of key chemical species simulated using the box and LES approaches are apparent. In general, the LES results show much greater dynamically-driven variability, and with some net deviations from the within-canyon mixing ratios taken from the box model. For NO, over the final 60 minutes of the simulation, the box model results are around 1 % higher than those of the LES simulation. Levels of NO_2 are also higher in the box model than the LES, throughout the simulation, with a mean difference of 10 % over the final hour of the modelled period ($150 \leq t \leq 210$ min), while ozone levels are correspondingly lower, by 6 % over the final hour of the simulation. Fig. 8(a) illustrates the change in mixing ratio of NO_x and O_X over time. Over the final hour of the model run, levels of NO_x and O_X simulated by the box model are higher than those from the LES by 3 and 8 % respectively (Table 3) – thus the changes in abundance reflect chemical impacts upon NO_x and O_X abundance, rather than solely perturbations to the $NO\text{-}NO_2\text{-}O_3$ photochemical steady state partitioning. Following the initial spin up of each model run, a large initial peak in both OH and HO_2 is observed directly after emissions are introduced. These peaks are followed by a rapid decline to equilibrium, which is achieved *ca*. 30 minutes after emission initiations. In contrast to the LES, the box model simulations approach equilibrium much more rapidly, reflecting the slower mixing processes inherent in the LES when compared to the fast and perfectly mixed conditions of the box model – as would be expected, segregation effects cause a reduction in the rate at which canyon-averaged concentrations approach the equilibrium levels simulated in a single-compartment model, i.e. street canyons respond more slowly to perturbations than a single-box model would suggest. OH and HO_2 levels simulated by the box model in steady state are higher than those in the LES simulation, with mean differences of 11 % and 8 % respectively over the final 60 minutes of the simulation. The assumption of instant mixing inherent to the box model leads to overestimates of the concentrations of NO, NO_2 and OH, and an underestimate for O_3, relative to the LES-RCS approach. Segregation effects, spatial inhomogeneity in composition due to incomplete mixing, reduce the canyon-averaged rate at which O_3 reacts with NO to produce NO_2 (i.e. the dominant pathway for NO to NO_2 conversion), due to limited or near-zero quantities of O_3 in a number of cells within the LES model domain, as is apparent in Fig. 3. In terms of HO_x, it is clear that segregation effects also play an important role in determining composition; the higher OH abundance within the box model implies an overestimate of the extent of OH-driven processing of reactive emissions within the canyon, compared with the more accurate LES scheme. While the comparison shown in Fig. 8(b) suggests a deviation of the order of 11 %, the actual difference will be greater, as the OH levels experienced by the majority of emitted air parcels within the canyon will reflect the circumference of the vortex, rather than the centre (where OH levels are approximately 30 % higher).

4.4 VOC oxidation chemistry and atmospheric composition: RCS v a simple chemistry case

To further ascertain the effect of the detailed VOC oxidation chemistry, the results obtained using the RCS mechanism (51 chemical species and 136 reactions) were compared with those obtained using a 3 reaction scheme (O_3-NO_x chemistry alone, *i.e.* reactions 8 - 10, below), as used by previously by Baik et al. (2007), Baker et al. (2004) and Grawe et al. (2007).

$$NO_2 + h\nu \longrightarrow NO + O; \quad (8)$$

$$O + O_2 + M \longrightarrow O_3 + M; \quad (9)$$

$$NO + O_3 \longrightarrow NO_2 + O_2. \quad (10)$$

Comparisons were performed using both the LES and box-model dynamical frameworks. The initial conditions (NO_x and O_3 levels) were identical to those applied using the full chemical scheme in both cases, and within the LES construct the simulated dynamics were identical to those used with the full chemical scheme. It is important to note that photochemical steady state was not in fact achieved (or assumed) in any cells of the model domain – as the dynamical residence time was too short (typically fractions of a second, *vs*. the 1 - 2 minute time constant for the NO-NO_2-O_3 system under sunlit conditions). Fig. 9 shows a comparison of the O_3-NO_x-only case with the full RCS reaction scheme. Going from the simple to the full scheme, levels of NO_2 and O_3 are higher and NO lower, reflecting additional NO to NO_2 conversion (and net ozone production) in the more detailed chemistry. Correspondingly, levels of O_x are higher, while NO_x levels are slightly lower (again, going from the simple to the full scheme), reflecting the presence of NO_x loss processes (e.g. formation of nitric acid, HNO_3) and partitioning to other NO_y species (e.g. HONO, HO_2NO_2). The differences between the full RCS scheme, and O_3-NO_x-only case, are similar but not identical between the box and LES dynamical frameworks – the changes in NO, NO_2, NO_x, O_3 and O_x are all less between the two LES models (dashed lines in Fig. 9), than the two box models (solid lines in Figure 9). For example, for NO the box models show a decrease of ca. 8 % going from the O_3-NO_x-only to the full chemical approaches, while the reduction is only 5 % for the LES models. For NO_2, the corresponding increases are ca. 18 % for the box models and 12 % for the LES approaches; changes in ozone are (proportionately) similar. Within the LES dynamical framework, the system is less sensitive to the additional chemical processes included in the RCS, compared with the O_3-NO_x-only scheme. In much of the domain, O_3 levels are very low / zero, such that the NO:NO_2 ratio is increased, and impacts of NO_x removal and partitioning in the full chemical scheme are reduced, while ozone production is immediately repartitioned into NO_2 – effectively, segregation effects in the LES simulations make the canyon-averaged model composition less sensitive to the chemical simplifications attendant in moving from the RCS to the basic O_3-NO_x only chemical mechanism. These results are consistent with those of Garmory et al. (2009), who found only a modest sensitivity of the predicted NO_x and O_3 levels towards the level of detail in the chemical mechanism used, but do not agree with the findings of Kim et al. (2012), who reported substantial (> 100 %) changes in ozone levels with the inclusion of VOC oxidation chemistry, in comparison with an O_3-NO_x only type approach. It is surprising that Kim et al. observed such substantial increases in ozone, as observed photochemical ozone production

642 rates are typically of the order of 5-20 ppb per hour (e.g. Cazorla et al., 2012), so increases of the
643 order reported would imply canyon residence times of the order of hours. The study of Kim et al.
644 successfully reproduced observed levels of essentially conserved species such as CO, suggesting that
645 the general canyon circulation / residence time / ventilation rate were well simulated, but noted that
646 levels of NO were substantially greater than those observed, pointing to differences in emissions from
647 those occurring in reality – substantial discrepancies between predicted and observed vehicular
648 emissions, particularly for NO_x, are widely observed (e.g. Carslaw et al., 2011). Alternatively, this
649 may reflect different model approaches to implementing photochemical steady state within the model
650 – if it is assumed that photochemical steady state is actually achieved within each cell (in contrast to
651 the present work), a different distribution between NO + O_3 and NO_2 would result – one which,
652 relative to the approach used here, would be expected to favour NO_2 in the near-source region within
653 the canyon, and NO + O_3 in the canyon outlet. It is not clear from the descriptions given if
654 photochemical steady state was in fact adopted by Kim et al.
655
656 *4.5 Within-Canyon Chemical Processing*
657 Fig. 10 illustrates the change in mixing ratio of O_3, NO, NO_2, NO_x and O_X with height at the canyon
658 inlet (x/W = -0.5) and canyon outlet planes (x/W = +0.5). Increases are observed in the level of NO,
659 NO_2, NO_x and O_X leaving the canyon, indicating the combined effect of primary emissions and
660 chemical processing on the abundance of pollutants escaping to the wider background atmosphere. In
661 order to evaluate the extent of within-canyon processing further, the change in vertical flux of a
662 number of species with height was calculated based on Equation 5 for the final hour of the model
663 simulation (shown in Fig. 11). The calculated resolved-scale flux near roof level (z/H = 1) can be
664 used to determine a representative flux of pollutants out of the canyon and into the background
665 atmosphere. This may then be compared with raw emission rates to evaluate the within-canyon
666 processing (although given the turbulent nature of the canyon-background interface (e.g. Figs 1, 3) the
667 choice of height at which to evaluate this is somewhat arbitrary). A peak in the resolved-scale
668 turbulent flux profile is apparent at $z/H \approx 0.1$ and a decrease in total flux is seen for $z/H < 0.1$ in all
669 flux profiles. This is the result of the elevation of the line emission source located within the centre of
670 the canyon 1 m above street level. For the passive scalar, the profile differs from that expected a priori
671 for a conserved quantity which should remain constant with height. At roof level ($z/H \approx 1$) the flux of
672 the passive scalar into the background atmosphere is equal to 933 ppb m^{-2} s^{-1} i.e. 93 % of that emitted
673 is escaping into the wider atmosphere. The maximum flux of the passive scalar of 1000 ppb m^{-2} s^{-1} is
674 observed slightly below roof level. This observed decrease in the flux of passive scalar with height
675 arises from the sub-grid scale turbulent dispersion not resolved explicitly within the LES model (the
676 sub-grid scale flux is not included here). Because of this, the fluxes of NO_x and O_X out of the canyon
677 discussed below are obtained at a height slightly below the roof level, z_f = 0.933 H, where the

678 contribution of sub-grid scale dispersion is minimised and at which height the flux of passive scalar
679 reaches 99.6% of its theoretical value.
680
681 A positive upward total flux of both NO and NO_2 from within the street to the overlying background
682 atmosphere is observed with a negative (downward) flux of O_3, with a significant effect of within-
683 canyon chemical processing upon pollutant flux escaping the canyon apparent for NO and NO_2. The
684 maximum total flux of NO (798 ppb m^{-2} s^{-1}) occurs near street level ($z/H \approx 0.2$). At $z = z_f$, the flux of
685 NO is equal to 752 ppb m^{-2} s^{-1} compared to a raw emission rate equivalent to 900 ppb s^{-1}. Therefore
686 there is an approximately 16.5 % chemical conversion of NO within the canyon when compared to the
687 raw emission rate. The maximum flux of NO_2 (248 ppb m^{-2} s^{-1}) occurs just below roof level and is
688 approximately 2.5 times that of the raw emission rate of 100 ppb s^{-1}, again indicating within-canyon
689 processing affecting the level of NO_2 escaping into the wider urban boundary layer. In terms of O_3
690 the maximum downward flux into the canyon of 135 ppb m^{-2} s^{-1} occurs just above roof level as O_3
691 rich background air enters the canyon from above, and O_3 is removed within the canyon by reaction
692 with NO. At $z = z_f$ (near roof level), the flux of NO_x is 989 ppb m^{-2} s^{-1} or 1.1% lower than that
693 emitted; O_X is 130 ppb m^{-2} s^{-1} at $z = z_f$, or 30% higher than the 100 ppb s^{-1} of NO_2 emitted. Therefore
694 NO_x release into the boundary layer is almost the same as that emitted, but oxidant release increases
695 significantly, in part as a result of the chemical processing taking place within the canyon. These
696 findings demonstrate the value in considering the modelled (and observed) levels of NO_x and of
697 oxidant (O_x), alongside NO / NO_2 / O_3, which can be used to disaggregate the effects of NO_x-O_3
698 photochemical steady state from net photochemical ozone production. Garmory et al. (2009) report
699 values of simulated OH levels along a vertical profile through the centre of the canyon of the order of
700 0.003 – 0.006 ppt, significantly lower than the mean within-canyon value determined here (0.08 ppt;
701 Table 3); however differences in the emissions profiles (total NO_x emission used here *ca*. 60 % of that
702 of Garmory et al. (with differing fractions of primary NO_2: 5 % vs. 1 % respectively), and a much
703 lower VOC:NO_x emission ratio (*ca*. 10 % of that used by Garmory et al., by volume, excluding CO)
704 probably accounts for much of this difference – lower OH levels reflecting the much larger VOC sink,
705 not compensated for by equivalently enhanced NO-driven HO_x cycling. Kim et al. (2012) showed
706 that OH-driven oxidation (of SO_2 and NO_2) could result in measurable secondary aerosol production
707 of up to 0.7 μg m^{-3} within the street canyon, which may be compared with roadside PM_{10} levels of 25
708 – 47 μg m^{-3} (whole UK roadside site annual average, and Marylebone roadside annual average -
709 AQEG, 2005). Kim et al. do not report their simulated OH levels, and no condensed phase processes
710 were considered in this work; however an upper estimate for comparison may be obtained: The mean
711 flux through the OH + NO_2 reaction (Table 2, *i.e.* neglecting that only a fraction of this will partition
712 to the particulate phase within the canyon) equates to 56 μg m^{-3} of HNO_3 production, supporting the

conclusion of Kim et al. that significant secondary aerosol production may occur on the canyon timescale.

Several studies have examined the partition of total flux of a scalar (F_{total}) between mean advective flux (F_{adv}) and turbulent flux (F_{turb}) for a street canyon. Based on the results of their RANS renormalisation group (RNG) k-ε turbulence model for a passive scalar, Liu et al. (2011) analysed roof level fluxes, *i.e.*, $F(z=H)$, where $F(z)$ as defined by Equation 5 can be either F_{adv} or F_{turb} (denoted by $\overline{PCH}$ or *PCH"* in their paper). Our results (Fig. 11) demonstrate that both $F_{adv}(z)$ or $F_{turb}(z)$ are very sensitive to height near the roof level. The 2D fields of $F_{adv}(x,z)$ and $F_{turb}(x,z)$ for a passive scalar derived from LES simulations conducted by Cheng and Liu (2011) support this observation. Therefore the analysis of vertical profiles of F_{adv} and F_{turb} is necessary and useful. As seen in Fig. 11, the dominant vertical flux observed within the canyon from the street level up to $z/H \approx 0.8$ is the mean advective flux which transports all pollutants (except for O_3) upwards toward roof level throughout the canyon. Between $z/H \approx 0.8$ and roof level, the mean advective flux decreases rapidly to become negative just above the top of the canyon ($1.0 \leq z/H \leq 1.2$) indicating that the mean flow (averaged across the domain) acts to entrain pollutants downwards toward the canyon at this height. For all species included in Fig. 11, a large increase in the resolved-scale turbulent flux is observed toward roof level indicating the importance of the shear layer associated turbulent processes in pollutant exchange at this level. For all species except O_3, the resolved-scale turbulent flux at roof level is at a maximum and is positive, indicating that there is more pollutant escaping out of the canyon at this height through turbulent transport than entering from the background atmosphere above. The mean flux of all species excluding O_3 and O_X becomes close to zero at a height of $z/H \approx 1.4$ i.e. toward the free flowing boundary layer above, which is unaffected by the dynamical processes taking place within and just above the canyon itself. For O_3 however, a negative mean flux is observed until well above roof level indicating net downward transport of O_3 rich air towards the canyon. These results are consistent with those of Baik et al. (2007), who adopted an RNG k-ε turbulence model but applied it to simple NO_x-O_3 chemistry; they showed 2D fields of $-\partial F(x,z)/\partial z$ instead of $F(x,z)$ for the purpose of budget analysis, in which $F(x,z)$ was either $F_{adv}(x,z)$ or $F_{turb}(x,z)$ of NO, NO_2, and O_3.

5. Conclusions

A reduced chemical scheme has been developed based upon a subset of a near explicit chemical mechanism, and implemented within an LES simulation of urban street canyon dynamics. The resultant LES-RCS model has been used to investigate urban street canyon atmospheric composition by simulating the combined effects of emissions, mixing and chemical processing on pollutant concentration within an idealised canyon. Pollutants within and above the canyon were found to show a clear spatial variation, with NO_x levels close to the leeward wall over double those of the

windward wall; such variations are of importance in assessing the potential exposure of receptors to air pollutants. Through comparison of simulations using the LES dynamical framework with those using a simple zero-dimensional box model approach, the effects of segregation on canyon atmospheric chemistry and composition are evident. Compared with a single-box canyon model, the LES scheme responds more slowly to chemical perturbations, and (after quasi-equilibrium is established) the box model simulated levels of NO, NO_2 and OH were found to be higher than their (canyon-averaged) equivalents in the more realistic LES scheme, while levels of O_3 were underestimated compared with the LES approach. The assumption of instant mixing inherent to the box model leads to overestimates of the concentrations of NO, NO_2 and OH, and an underestimate for O_3, relative to the LES approach. Segregation effects, due to spatial inhomogeneity in composition due to incomplete mixing, reduce the canyon-averaged rate at which O_3 reacts with NO to produce NO_2 (i.e. the dominant pathway for NO to NO_2 conversion), due to limited quantities of O_3 present in a number of cells within the LES model domain (Fig. 3). Segregation effects also affect HO_x levels; the higher OH abundance within the box model implies an overestimate of the extent of OH-driven processing of reactive emissions within the canyon, compared with the more realistic LES approach. While the comparison shown in Fig. 8(b) suggests a deviation of the order of 11 %, the actual difference will be greater, as the OH levels experienced by the majority of emitted air parcels within the canyon will reflect the circumference of the vortex, rather than the centre (where OH levels are approximately 30 % higher). Through comparison of the comprehensive RCS and O_3-NO_x-only chemical mechanisms, a clear effect of the inclusion of detailed oxidation chemistry is also evident. Going from the O_3-NO_x only system to the RCS mechanisms, levels of NO_2 and O_3 are higher and NO lower, reflecting additional NO to NO_2 conversion (and net ozone production) under the more detailed chemistry. Segregation effects reduced the sensitivity of the model outputs to the increase in chemical complexity when comparing the box model dynamical framework to the LES approach.

Chemical processing of emissions takes place within the canyon, contributing to an increase in O_x (O_3 + NO_2) of 30 % (compared to the primary NO_2 component of the emission source), for the moderately polluted emission scenario considered. This result shows that the atmospheric "pre-processing" of primary emissions taking place within street canyons can be significant in terms of atmospheric composition and the flux of pollutants from street canyon level to the wider urban boundary layer above. These processes are likely to be dependent upon the nature of the domain (canyon aspect ratio), prevailing meteorology and emission / pollution scenario considered. Further research to average the extent of these effects across a representative parameter space will determine the modification to raw emission rates which might be applied to account for within canyon processing of raw emissions in larger scale regional and neighbourhood models.

Acknowledgements

The authors would like to thank Dr Mike Jenkin and Professor Dudley Shallcross for the provision of the Common Representatives Intermediates mechanism version 2-R5. VB thanks the University of Birmingham for award of a PhD scholarship. The computations described in this paper were performed using the University of Birmingham's BlueBEAR HPC service (http://www.bear.bham.ac.uk), which was purchased through HEFCE SRIF-3 funds. The comments of the anonymous reviewers are gratefully acknowledged.

795 **References**

796

797 AQEG, 2005. Particulate Matter in the United Kingdom. Report of the UK Air Quality
798 Expert Group, AQEG. Prepared for the Department for Environment, Food and Rural
799 Affairs, the Scottish Executive, the Welsh Assembly Government and the Department
800 of the Environment in Northern Ireland.
801 AQEG, 2009. Ozone in the United Kingdom. Report of the UK Air Quality Expert Group,
802 AQEG. Prepared for the Department for Environment, Food and Rural Affairs, the
803 Scottish Executive, the Welsh Assembly Government and the Department of the
804 Environment in Northern Ireland.
805 Aumont, B., Szopa, S., Madronich, S., 2005. Modelling the evolution of organic carbon
806 during its gas-phase tropospheric oxidation: development of an explicit model based on
807 a self generating approach. *Atmos. Chem. Phys*. **5**, 2497-2517.
808 Baik, J.J., Kang, Y.S., Kim, J.J., 2007. Modeling reactive pollutant dispersion in an urban
809 street canyon. *Atmospheric Environment* **41**, 934-949.
810 Baker, J., Walker, H.L., Cai, X.M., 2004. A study of the dispersion and transport of reactive
811 pollutants in and above street canyons - a large eddy simulation. *Atmospheric*
812 *Environment* **38**, 6883-6892.
813 Berkowicz, R., Ketzel, M., Vachon, G., Louka, P., Rosant, J.M., Mestayer, P.G., Sini, J.F.,
814 2002. Examination of traffic pollution distribution in a street canyon using the
815 Nantes'99 experimental data and comparison with model results, in: Sokhi, R.S.,
816 Bartzis, J.G. (Eds.), *Urban Air Quality - Recent Advances, Proceedings*, pp. 311-324.
817 Bey, I., Jacob, D.J., Yantosca, R.M., Logan. J.A., Field, B.D., Fiore, A.M., Li, Q., Liu, H.Y.,
818 Mickley, L.J., Schultz, M.G. 2001. Global modelling of tropospheric chemistry with
819 assimilated meteorology: model description and evaluation. *J. Geophys. Res.* **106**,
820 23073-23095.
821 Bloss, C., Wagner, V., Jenkin, M.E., Volkamer, R., Bloss, W.J., Lee, J.D., Heard, D.E.,
822 Wirtz, K., Martin-Reviejo, M., Rea, G., Wenger, J.C., Pilling, M.J., 2005. Development
823 of a detailed chemical mechanism (MCMv3.1) for the atmospheric oxidation of
824 aromatic hydrocarbons. *Atmos. Chem. Phys*. **5**, 641-664.
825 Boulter, P.G., Barlow, T.J., Latham, S., McCrae, I.S., 2009. Emission Factors 2009: Report 1
826 - a review of methods for determining hot exhaust emission factors for road vehicles.
827 TRL, Wokingham.

828 Cai, X.M., Barlow, J.F., Belcher, S.E., 2008. Dispersion and transfer of passive scalars in and
829 above street canyons - Large-eddy simulations. *Atmospheric Environment* **42**, 5885-
830 5895.
831 Carslaw, D., Beevers, S., Westmoreland, E., Williams, M., Tate, J., Murrells, T., Stedman, J.,
832 Li, Y., Grice, S., Kent, A., Tsagatakis, I., 2011. Trends in NO_x and NO_2 emissions and
833 ambient measurements in the UK, *Department for Environment Food and Rural*
834 *Affairs.*
835 Cazorla, M., Brune, W.H., Lefer, B. 2012. Direct measurement of ozone production rates in
836 Houston in 2009 and comparison with two estimation methods, *Atmos. Chem. Phys.* **12**,
837 1205-1212.
838 Cheng, W., Liu, C.-H., 2011. Large-Eddy Simulation of Flow and Pollutant Transports in and
839 Above Two-Dimensional Idealized Street Canyons. *Boundary-Layer Meteorology*, 1-
840 27.
841 Cheng, W., Liu, C.-H., 2011. Large-eddy simulation of turbulent transports in urban street
842 canyons in different thermal stabilities, *J. Wind Engineering Ind. Aerodyn.,* **99,** 434-
843 442.
844 Cui, Z.Q., Cai, X.M., Baker, C.J., 2004. Large-eddy simulation of turbulent flow in a street
845 canyon. *Quarterly Journal of the Royal Meteorological Society* **130**, 1373-1394.
846 DePaul, F.T., Sheih, C.M., 1985. A tracer study of dispersion in an urban street canyon.
847 *Atmospheric Environment* (1967) **19**, 555-559.
848 DFT, 2009. Transport Statistics Bulletin, Road Statistics 2008: Traffic, Speeds and
849 Congestion. Department for Transport.
850 Dodge, M.C., 2000. Chemical oxidant mechanisms for air quality modeling: critical review.
851 *Atmospheric Environment* **34**, 2103-2130.
852 Emmerson, K.M., Evans, M.J., 2009. Comparison of tropospheric gas-phase chemistry
853 schemes for use within global models. *Atmos. Chem. Phys*. **9**, 1831-1845.
854 Garmory, A., Richardson, E.S., Mastorakos, E., 2006. Micromixing effects in a reacting
855 plume by the Stochastic Fields method. *Atmospheric Environment* **40**, 1078-1091.
856 Garmory, A., Kim, I.S., Britter, R.E., Mastorakos, E., 2009. Simulations of the dispersion of
857 reactive pollutants in a street canyon, considering different chemical mechanisms and
858 micromixing. *Atmospheric Environment* **43**, 4670-4680.
859 Gery, M.W., Whitten, G.Z., Killus, J.P., Dodge, M.C., 1989. A photochemical kinetics
860 mechanism for urban and regional scale computer modeling. *J. Geophys. Res.-Atmos.*
861 **94**, 12925-12956.

862 Grawe, D., Cai, X.M., Harrison, R.M., 2007. Large eddy simulation of shading effects on
863 NO2 and O-3 concentrations within an idealised street canyon. *Atmospheric*
864 *Environment* **41**, 7304-7314.
865 Gromke, C., Buccolieri, R., Di Sabatino, S., Ruck, B., 2008. Dispersion study in a street
866 canyon with tree planting by means of wind tunnel and numerical investigations -
867 Evaluation of CFD data with experimental data. *Atmospheric Environment* **42**, 8640-
868 8650.
869 Heard, D.E., Pilling, M.J., 2003. Measurement of OH and HO2 in the troposphere. *Chem.*
870 *Rev.* **103**, 5163-5198.
871 Hunter, L.J., Johnson, G.T., Watson, I.D., 1992. An investigation of three-dimensional
872 characteristics of flow regimes within the urban canyon. *Atmospheric Environment*.
873 Part B. Urban Atmosphere **26**, 425-432.
874 Jenkin, M.E., Saunders, S.M., Pilling, M.J., 1997. The tropospheric degradation of volatile
875 organic compounds: A Protocol for Mechanism Development, *Atmospheric*
876 *Environment* 31, 81-104.
877 Jenkin, M.E., Saunders, S.M., Wagner, V., Pilling, M.J., 2003. Protocol for the development
878 of the Master Chemical Mechanism, MCM v3 (Part B): tropospheric degradation of
879 aromatic volatile organic compounds. *Atmos. Chem. Phys*. **3,** 181-193.
880 Jenkin, M.E., Watson, L.A., Utembe, S.R., Shallcross, D.E., 2008. A Common
881 Representative Intermediates (CRI) mechanism for VOC degradation. Part 1: Gas phase
882 mechanism development. *Atmospheric Environment* **42**, 7185-7195.
883 Kastner-Klein, P., Plate, E.J., 1999. Wind-tunnel study of concentration fields in street
884 canyons. *Atmospheric Environment* **33**, 3973-3979.
885 Kim, M.J., Park, R.J., Kim, J.-J. 2012. Urban air quality modelling with full O_3-NO_x-VOC
886 chemistry: Implications for O_3 and PM air quality in a street canyon. *Atmos. Environ.*
887 **47**, 330-340.
888 Krol, M.C., Molemaker, M.J., de Arellano, J.V.G., 2000. Effects of turbulence and
889 heterogeneous emissions on photochemically active species in the convective boundary
890 layer. *J. Geophys. Res.-Atmos*. **105**, 6871-6884.
891 Kwak, K.-H., Baik, J.-J. 2012. A CFD modeling study of the impacts of NO_x and VOC
892 emissions on reactive pollutant dispersion in and above a street canyon. *Atmos.*
893 *Environ.* **46**, 71-80.
894 Lee, J.D., Lewis, A.C., Monks, P.S., Jacob, M., Hamilton, J.F., Hopkins, J.R., Watson, N.M.,
895 Saxton, J.E., Ennis, C., Carpenter, L.J., Carslaw, N., Fleming, Z., Bandy, B.J., Oram,

D.E., Penkett, S.A., Slemr, J., Norton, E., Rickard, A.R., Whalley, L.K., Heard, D.E., Bloss, W.J., Gravestock, T., Smith, S.C., Stanton, J., Pilling, M.J., Jenkin, M.E., 2006. Ozone photochemistry and elevated isoprene during the UK heatwave of August 2003. *Atmospheric Environment* **40**, 7598-7613.

Li, X.-X., Liu, C.-H., Leung, D., 2008. Large-Eddy Simulation of Flow and Pollutant Dispersion in High-Aspect-Ratio Urban Street Canyons with Wall Model. *Boundary-Layer Meteorology* **129**, 249-268.

Li, X.-X., Liu, C.H., Leung, D.Y.C., 2009. Numerical investigation of pollutant transport characteristics inside deep urban street canyons. *Atmospheric Environment* **43**, 2410-2418.

Li, X.X., Liu, C.H., Leung, D.Y.C., Lam, K.M., 2006. Recent progress in CFD modelling of wind field and pollutant transport in street canyons. *Atmospheric Environment* **40**, 5640-5658.

Liu, C.-H., Cheng, W.C., Leung, T.C.Y., Leung, D.Y.C., 2011. On the mechanism of air pollutant re-entrainment in two-dimensional idealized street canyons. *Atmospheric Environment* **45**, 4763-4769.

Liu, C.H., Barth, M.C., 2002. Large-eddy simulation of flow and scalar transport in a modeled street canyon. *J. Appl. Meteorol*. **41**, 660-673.

Liu, C.H., Barth, M.C., Leung, D.Y.C., 2004. Large-eddy simulation of flow and pollutant transport in street canyons of different building-height-to-street-width ratios. *J. Appl. Meteorol.* **43**, 1410-1424.

Lelieveld, J., Butler, T.M., Crowley, J.N., Dillon, T.J., Fischer, H., Ganzeveld, L., Harder, H., Lawrence, M.G., Martinez, M., Taraborrelli, D. and Williams, J., 2008. Atmospheric oxidation capacity sustained by a tropical forest. *Nature* **452**, 736-740.

Louka, P., Belcher, S.E., Harrison, R.G., 2000. Coupling between air flow in streets and the well-developed boundary layer aloft. *Atmospheric Environment* **34**, 2613-2621.

Madronich, S., Flocke, S., 1998. The role of solar radiation in atmospheric chemistry in: Boule, P. (Ed.), Handbook of Environmental Chemistry. Springer, New York, pp. 1–26.

Oke, T.R., 1987. Boundary layer climates / T.R. Oke, 2nd ed. Methuen, London.

Pavageau, M., Schatzmann, M., 1999. Wind tunnel measurements of concentration fluctuations in an urban street canyon. *Atmospheric Environment* **33**, 3961-3971.

Pugh, T.A.M., MacKenzie, A.R., Langford, B., Nemitz, E., Misztal, P.K., Hewitt, N.K., 2011. The influence of small-scale variations in isoprene concentrations on atmospheric chemistry over a tropical rainforest, *Atmos. Chem. Phys.* **11**, 4121-4134

930 Salim, S.M., Buccolieri, R., Chan, A., Di Sabatino, S., 2010. Numerical simulation of
931 atmospheric pollutant dispersion in an urban street canyon: Comparison between
932 RANS and LES. *Journal of Wind Engineering and Industrial Aerodynamics* **99**, 103-
933 113.
934 Salizzoni, P., Soulhac, L., Mejean, P., 2009. Street canyon ventilation and atmospheric
935 turbulence. *Atmospheric Environment* **43**, 5056-5067.
936 Saunders, S.M., Jenkin, M.E., Derwent, R.G., Pilling, M.J., 2003. Protocol for the
937 development of the Master Chemical Mechanism, MCM v3 (Part A): tropospheric
938 degradation of non-aromatic volatile organic compounds. *Atmos. Chem. Phys*. **3**, 161-
939 180.
940 So, E.S.P., Chan, A.T.Y., Wong, A.Y.T., 2005. Large-eddy simulations of wind flow and
941 pollutant dispersion in a street canyon. *Atmospheric Environment* **39**, 3573-3582.
942 Tomlin, A.S., Smalley, R.J., Tate, J.E., Barlow, J.F., Belcher, S.E., Arnold, S.J., Dobre, A.,
943 Robins, A., 2009. A field study of factors influencing the concentrations of a traffic-
944 related pollutant in the vicinity of a complex urban junction. *Atmospheric Environment*
945 **43**, 5027-5037.
946 Vardoulakis, S., Fisher, B.E.A., Pericleous, K., Gonzalez-Flesca, N., 2003. Modelling air
947 quality in street canyons: a review. *Atmospheric Environment* **37**, 155-182.
948 Wang, P., Mu, H.L., 2010. Analysis of Reactive Pollutants Distribution in Damaging Street
949 Canyon Architectures, in: Luo, Q. (Ed.), *Information Technology for Manufacturing*
950 *Systems*, Pts 1 and 2, pp. 1115-1120.
951 Watson, L.A., Shallcross, D.E., Utembe, S.R., Jenkin, M.E., 2008. A Common
952 Representative Intermediates (CRI) mechanism for VOC degradation. Part 2: Gas phase
953 mechanism reduction. *Atmospheric Environment* **42**, 7196-7204.
954 Xie, S.D., Zhang, Y.H., Li, Q., Tang, X.Y., 2003. Spatial distribution of traffic-related
955 pollutant concentrations in street canyons. *Atmospheric Environment* **37**, 3213-3224.

Figure 1

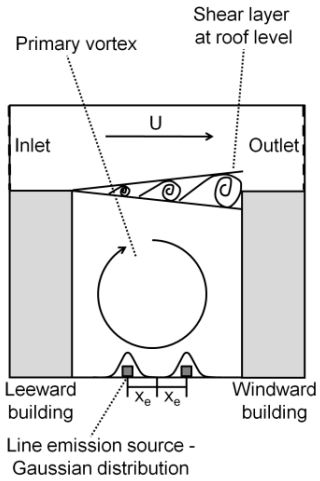

Fig. 1. Schematic diagram illustrating the main components of an idealised street canyon, as used in this study.

Figure 2

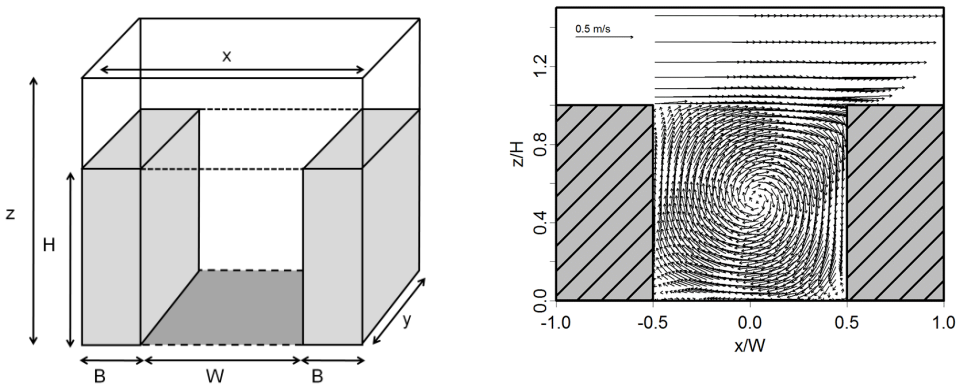

Fig. 2. (a) Schematic illustration of the LES model domain where x = 24 m, y = 40 m and z = 94 m with canyon dimensions W = 18 m, H = 18 m and B = 3 m and (b) Mean flow field diagram, showing temporally and spatially (along the y axis) averaged wind vectors (u, w). Averages were taken over the final hour of the model simulation ($150 \leq t \leq 210$ min), when the canyon circulation was fully developed.

Figure 3

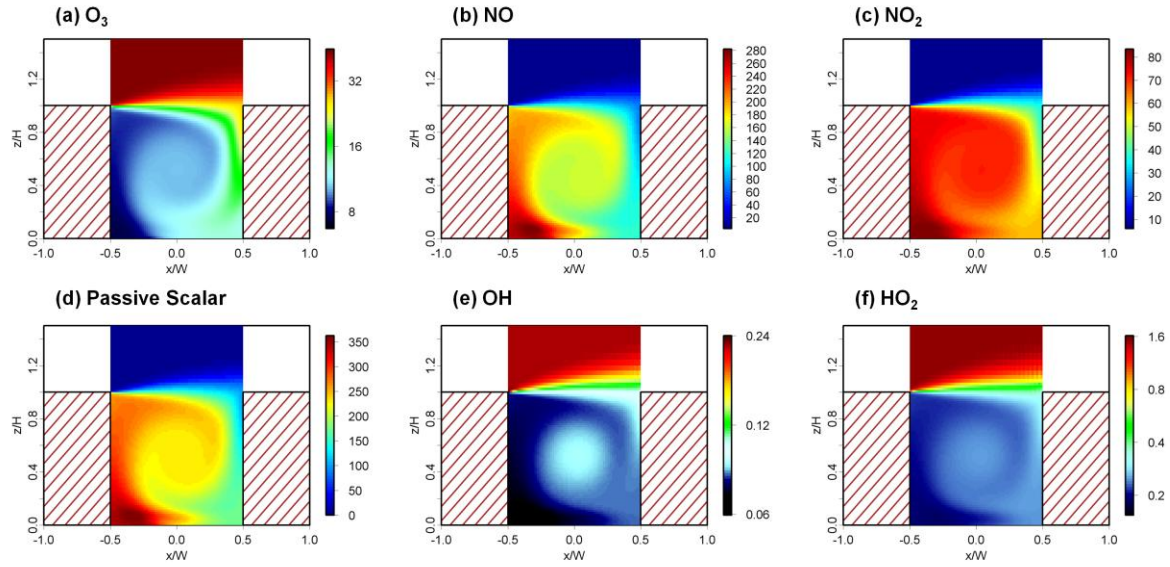

Fig. 3. Mean (time averaged) mixing ratios (ppb) of (a) O_3, (b) NO, (c) NO_2, (d) passive scalar, (e) OH (ppt) and (f) HO_2 (ppt) from the LES-RCS simulations. Data averaged over the final hour of the model simulation ($150 \leq t \leq 210$ min).

Figure 4

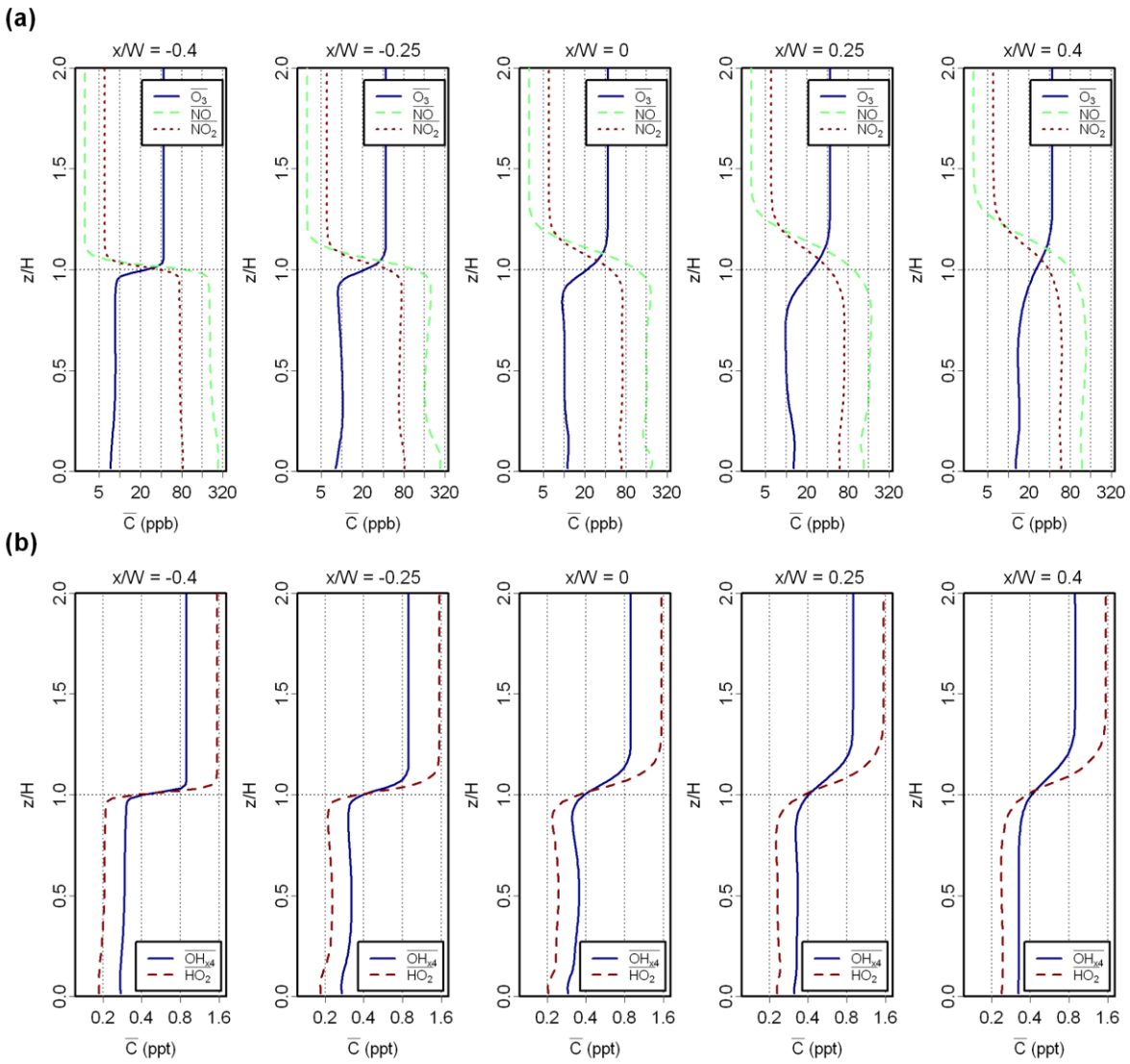

Fig. 4. Variation in the mean and time averaged mixing ratios of (a) O_3, NO, NO_2, and (b) OH_{x4} (4 × OH) and HO_2 with height within the canyon ($0.0 \leq z/H \leq 2.0$) at x/W= -0.4, 0.25, 0.0, 0.25, 0.4, from the LES-RCS simulation.

Figure 5

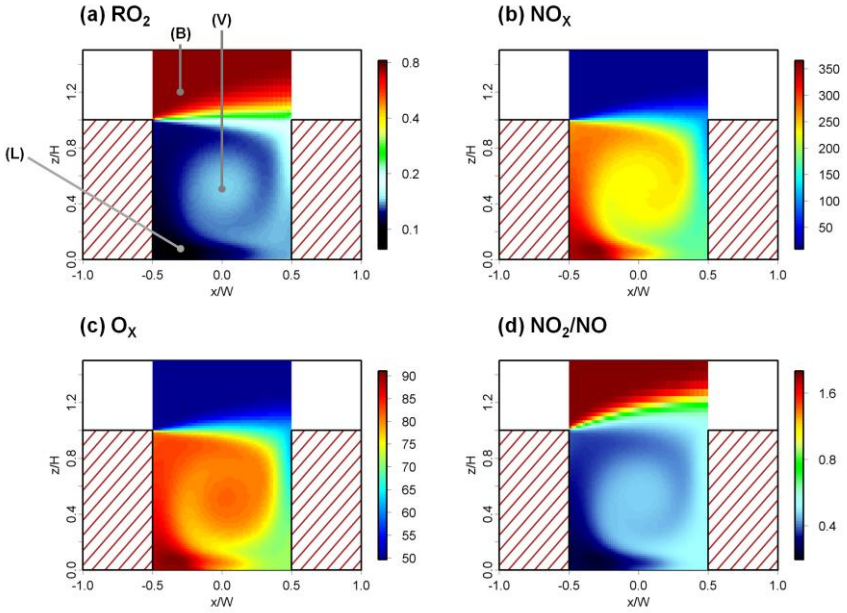

Fig. 5. Mean and time averaged mixing ratios of (a) RO_2 (ppt), (b) NO_x (ppb), (c) O_X (ppb) and (d) NO_2/NO ratio from the LES-RCS simulation.

Figure 6

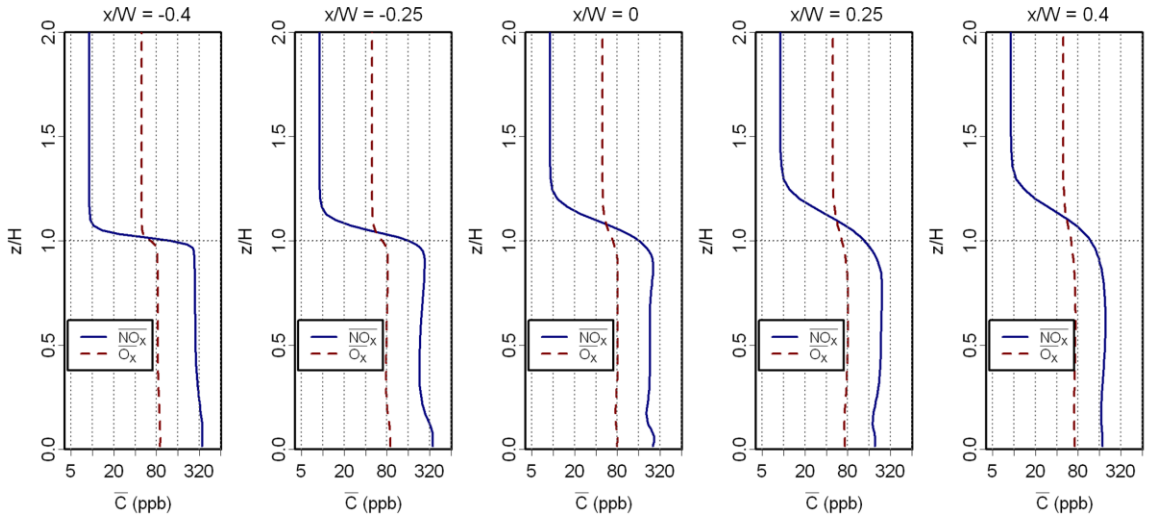

Fig. 6. Time averaged vertical mixing ratio profiles on a logarithmic scale of NO_x and O_X at x/W= -0.4, -0.25, 0.0, 0.25, 0.4 within and above the canyon ($0.0 \leq z/H \leq 2.0$), from the LES-RCS simulation.

Figure 7

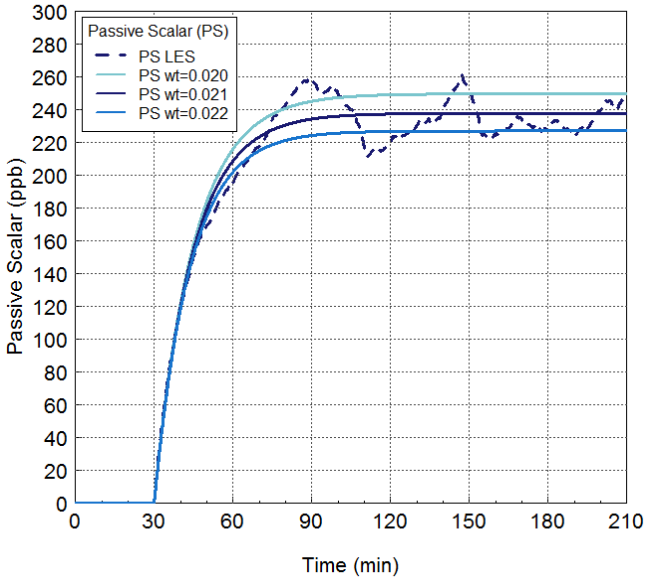

Fig. 7. Time evolution of the canyon averaged mixing ratio of the (chemically conserved) passive scalar calculated using the LES and box model dynamical frameworks, as a function of the exchange velocity (ω_t) – values in ms^{-1}.

Figure 8

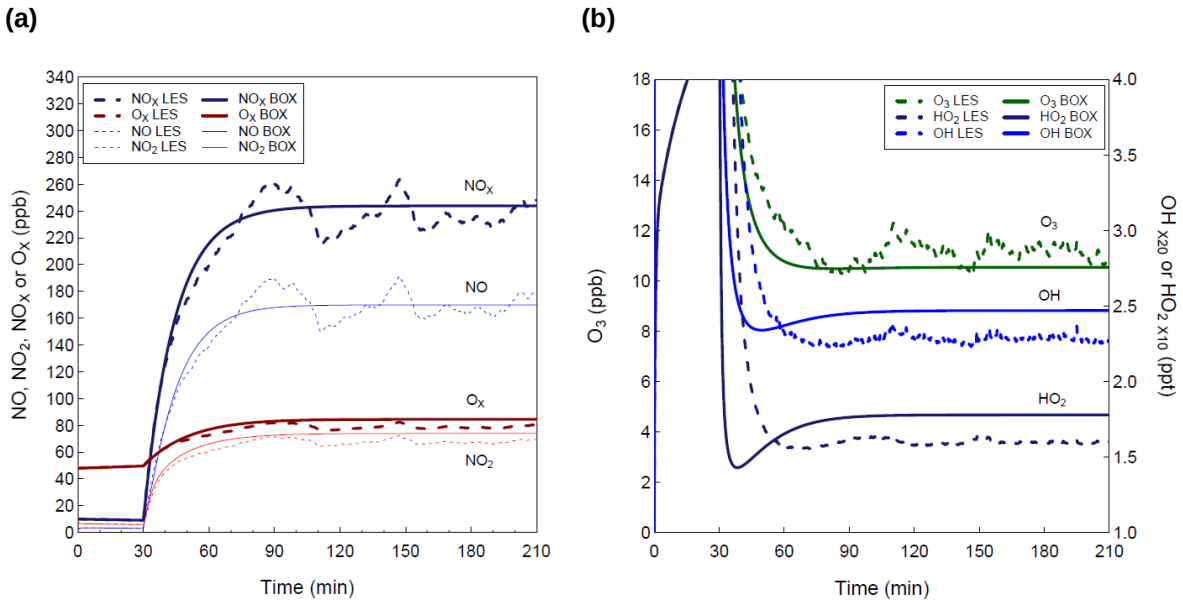

Fig. 8. Time evolution of the canyon averaged mixing ratio of (a) NO_x, O_X, NO, NO_2 (ppb) and (b) O_3 (ppb), OH_{x20} (20 × OH) (ppt), HO_{2x10} (10 × HO_2), calculated using the LES-RCS and Box-RCS simulations.

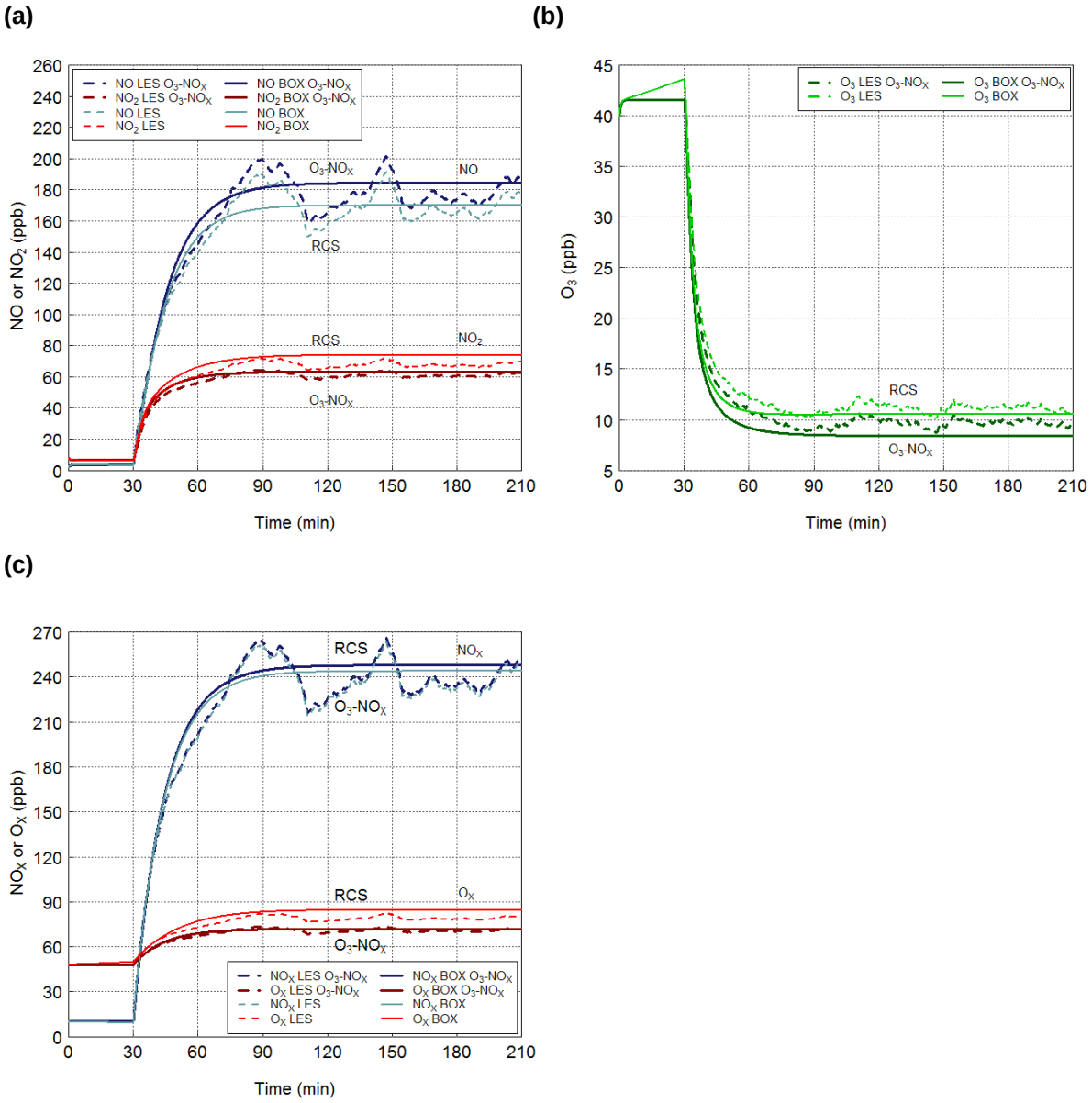

Fig. 9. Time evolution of canyon averaged mixing ratio (ppb) of (a) NO, NO_2; (b) O_3 and (c) NO_x, O_x, using the LES and box model dynamical frameworks, and the RCS and O_3-NO_x-only chemistry cases.

Figure 10

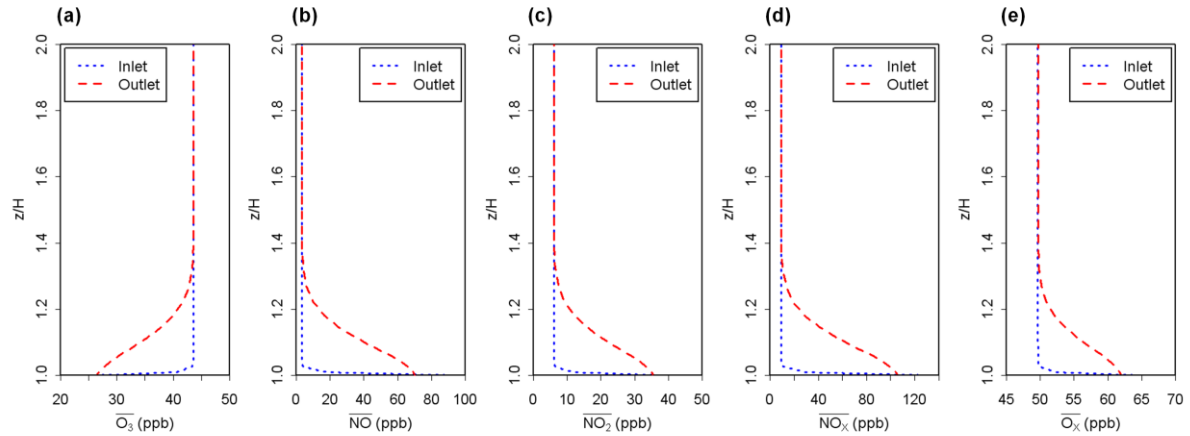

Fig. 10. Time averaged vertical mixing ratio profiles ($1.0 \leq z/H \leq 2.0$) of (a) O_3, (b) NO, (c) NO_2, (d) NO_x and (e) O_X (ppb) at the canyon inlet (x/W = -0.5) and canyon outlet (x/W = 0.5), from the LES-RCS simulations.

Figure 11

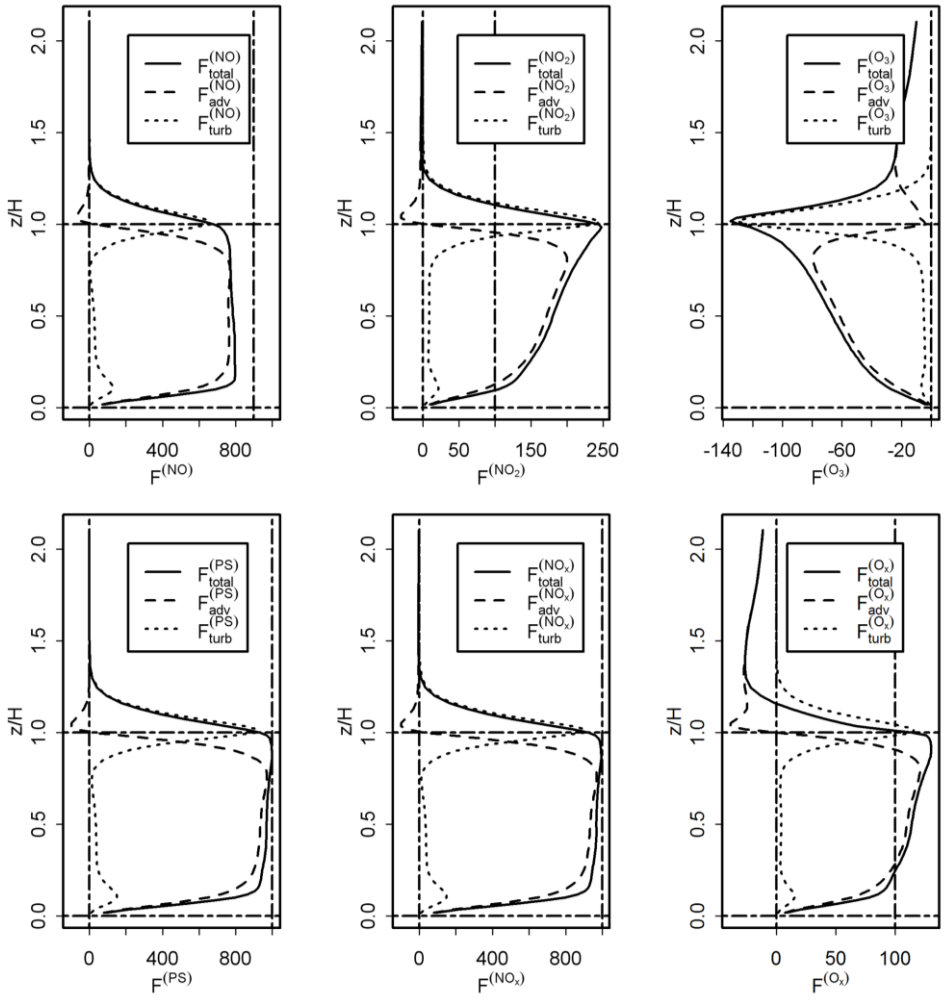

Fig. 11. Vertical profiles of advective, turbulent and total flux (ppb m^{-2} s^{-1}) averaged across the canyon ($-0.5 \leq x/W \geq 0.5$), from the LES-RCS simulation.

Table 1

Initial mixing ratios (ppb) used in the RCS model simulations

Species	Chemical formula	Mixing ratio / ppb
Nitric oxide	NO	2
Nitrogen dioxide	NO_2	8
Ozone	O_3	40
Carbon monoxide	CO	200
Nitric acid	HNO_3	2
Methane	CH_4	1800
Water vapour	H_2O	2 %
VOCs		
Ethene	C_2H_4	0.91
Propene	C_3H_6	0.29
Formaldehyde	HCHO	3.14
Acetaldehyde	CH_3CHO	2.98
Isoprene	C_5H_8	0.28
Methanol	CH_3OH	7.38
Ethanol	C_2H_5OH	2.37
Peroxyacetyl nitrate	PAN	0.46

Table 2

The dominant OH production and loss rates calculated for the LES-RCS simulation. Average concentrations taken over the final hour of the model simulation ($150 \leq t \leq 210$ min) and at three locations (Fig. 5): within the canyon vortex (V), toward the lower leeward wall (L) and in the background atmosphere (B).

	(V) Vortex	(L) Lower leeward wall	(B) Background atmosphere
	Rate of production / loss (ppt s^{-1})		
Production			
$HO_2 + NO \longrightarrow OH + NO_2$	100	174	4.8
$HONO + h\nu \longrightarrow OH + NO$	27	25	0.74
$O_3 + h\nu \longrightarrow OH + OH$	0.79	0.78	1.3
$O_3 + VOC \longrightarrow OH + products$	0.35	0.57	0.0060
Loss			
$OH + VOC \longrightarrow products$	-61	-96	-2.8
$OH + NO \longrightarrow HONO$	-41	-71	-0.78
$OH + NO_2 \longrightarrow HNO_3$	-22	-26	-1.9
$OH + CO \longrightarrow HO_2$	-5.0	-7.4	-1.0

Table 3

Canyon- and time-averaged mixing ratios calculated using the LES-RCS and Box-RCS model approaches

	(a) LES	(b) Box	(b) - (a)	[(b) - (a)] / (a)
	Mixing ratio (ppb)			%
O_3	11.2	10.5	-0.7	-5.9
NO	168	170	2	1.2
NO_2	68	74	6	9.5
OH*	0.08	0.09	0.01	11.3
HO_2*	0.23	0.25	0.02	8.1
NO_x	236	244	8	3.3
O_X	79	85	6	8.0
NO_2/NO	0.40	0.44		

*Mixing ratios of OH and HO_2 are given in ppt.

Table 4

Effect of exchange velocity: canyon and time averaged mixing ratios for the Box-RCS simulation with ω_t = 0.021m s^{-1} and ω_t = 0.022 m s^{-1}.

	(a) Box ω_t = 0.021 m s^{-1}	(b) Box ω_t = 0.022 m s^{-1}	(b) - (a)	[(b) - (a)] / (a)
	Mixing ratio (ppb)			%
O_3	10.54	10.76	0.22	2.1
NO	169.9	161.8	-8	-4.8
NO_2	74.0	71.6	-2	-3.2
OH*	0.089	0.088	-0.0012	-1.3
HO_2*	0.247	0.246	-0.0006	-0.3
NO_x	244	233	-11	-4.5
O_X	85	82	-3	-3.5

*Mixing ratios of OH and HO_2 are given in ppt.

Table 5

Comparison of mean (canyon- and time-averaged) mixing ratios, for the RCS and O_3-NO_x-only mechanisms, using the LES and Box model dynamical frameworks. .

	(a) LES RCS	(b) Box RCS	(c) LES O_3-NO_x	(d) Box O_3-NO_x	[(a) - (c)] / (c)	[(b) - (d)] / (d)
	Mixing ratio (ppb)				%	
O_3	11.2	10.5	9.7	8.4	15.5	25.0
NO	168	170	177	185	-5.1	-8.1
NO_2	68	74	61	63	11.5	17.5
NO_x	236	244	238	248	-0.8	-1.6
O_X	79	85	70.7	71.4	11.7	19.0
NO_2/NO	0.40	0.44	0.34	0.34		